Petroleum Science 21 (2024) 2048–2065

Contents lists available at ScienceDirect

Petroleum Science

journal homepage: www.keaipublishing.com/en/journals/petroleum-science

Original Paper

Influence of pressure disturbance wave on dynamic response characteristics of liquid film seal for multiphase pump

Qing-Ping Li [a, b], Jin-Ya Zhang [c, *], Jia-Xiang Zhang [c], Yong-Xue Zhang [c]

[a] CNOOC Research Institute Company Limited, Beijing, 100028, China
[b] State Key Laboratory of Natural Gas Hydrate, Beijing, 100028, China
[c] College of Mechanical and Transportation Engineering, China University of Petroleum, Beijing, 102249, China

ARTICLE INFO

Article history:
Received 20 November 2022
Received in revised form
16 November 2023
Accepted 16 November 2023
Available online 21 November 2023

Edited by Jia-Jia Fei

Keywords:
Multiphase pump
Liquid film seal
Pressure disturbance wave
Dynamic response characteristics

ABSTRACT

Slug flow or high GVF (Gas Volume Fraction) conditions can cause pressure disturbance waves and alternating loads at the boundary of mechanical seals for multiphase pumps, endangering the safety of multiphase pump units. The mechanical seal model is simplified by using periodic boundary conditions and numerical calculations are carried out based on the Zwart-Gerber-Belamri cavitation model. UDF (User Define Function) programs such as structural dynamics equations, alternating load equations, and pressure disturbance equations are embedded in numerical calculations, and the dynamic response characteristics of mechanical seal are studied using layered dynamic mesh technology. The results show that when the pressure disturbance occurs at the inlet, as the amplitude and period of the disturbance increase, the film thickness gradually decreases. And the fundamental reason for the hysteresis of the film thickness change is that the pressure in the high-pressure area cannot be restored in a timely manner. The maximum value of leakage and the minimum value of axial velocity are independent of the disturbance period and determined by the disturbance amplitude. The mutual interference between enhanced waves does not have a significant impact on the film thickness, while the front wave in the attenuated wave has a promoting effect on the subsequent film thickness changes, and the fluctuation of the liquid film cavitation rate and axial velocity under the attenuated wave condition deviates from the initial values. Compared with pressure disturbance conditions, alternating load conditions have a more significant impact on film thickness and leakage. During actual operation, it is necessary to avoid alternating load conditions in multiphase pump mechanical seals.

1. Introduction

Mechanical seals are widely used in rotating equipment (Necker, 2003), and the sealing principle is that when the fluid pressure acting on the axial direction is balanced with the elasticity of the compensation mechanism, a stable liquid film or gas film is formed in the gap due to the rotating effect of the moving ring to prevent leakage. The mechanical seal for multiphase pump shall be applicable to the special working environment of multiphase pump, that is, the fluctuation of IGVF, especially when the GVF of the inlet section of the pump is too high or the slug flow condition, it is very easy to cause a wide range of fluctuation of pressure in the pump. In addition, due to the influence of flow control, fluid excitation and other factors during actual operation, the pressure in the seal chamber will fluctuate regularly. During the operation of multiphase pump, the shaft system has radial and axial displacement and vibration, which forms complex alternating load at the mechanical seal. The unstable pressure at the boundary of the seal ring and the alternating load acting on the compensation ring surface are easy to cause uneven stress on both sides of the compensation ring, resulting in vibration. If it is serious, it may cause the seal end face to wear, damage the end face morphology, and reduce the sealing performance. Therefore, exploring the pressure fluctuation and alternating load is of great significance to the dynamic response characteristics and instantaneous sealing performance of the compensation ring, and provides a reference for predicting the vibration pattern of the mechanical seal for multiphase pump under complex working conditions for a long time.

* Corresponding author.
E-mail address: zhjinya@163.com (J.-Y. Zhang).

https://doi.org/10.1016/j.petsci.2023.11.018

At present, there are many researches on the cavitation characteristics of mechanical seals, mainly focusing on the cavitation experiment, cavitation mechanism, and the dynamic characteristics of mechanical seals. In the visual experiment of mechanical seal end face cavitation, Peng et al. (2019) summarized the research status of vapor-liquid two-phase end face mechanical seal in recent 50 years, summarized the typical heat source and heat transmission path of mechanical seal, expounded the phase change principle of mechanical seal, and summarized the measurement technology and method of end face fluid film parameters. Nau et al. (1980) and Xue et al. (2017) observed obvious cavitation areas in spiral groove rotating seals through experiments. Tokunaga et al. (2011) found that many micro hole areas were generated on the surface of the sealing ring, and the position of the hole area and the liquid flow path fluctuated with time. Zhou et al. (2016) conducted an experimental study on the lubrication characteristics of magnetic fluid film in spiral groove mechanical seals to reveal how the magnetic field affects the hydrodynamic effect of magnetic fluid. Rouillon et al. (2018) carried out the behavior and performance experiment of spiral groove mechanical end face seal in the application of liquid lubrication, and the results showed that the spiral groove end face seal has a larger working range, lower friction coefficient and higher leakage rate than the smooth end face seal. Li et al. (2020a, 2021) carried out forward and reverse rotation tests when the spiral groove was in the middle position, and established a hydrodynamic lubrication model with JFO cavitation boundary to study the cavitation in the sealing liquid film. Cochain et al. (2020) used numerical models and experimental devices to study the effects of end waviness and pressure reversal on mechanical seal leakage and external fluid entry. The research shows that the leakage decreases with the increase of spring force, and the leakage and external fluid entry increase with the increase of waviness amplitude.

In terms of cavitation mechanism of mechanical seal end face, Zeus et al. (1993) studied the necessary conditions for the formation of cavitation. Etison et al. (1996) and Findley et al. (1968) believed that the bearing capacity of the liquid film formed by cavitation could reduce the friction between end faces and achieve cavitation drag reduction. Meng et al. (2017, 2018) based on the theory of liquid lubrication and the small disturbance method, established the control equation of seal perturbation film pressure considering liquid film cavitation. The finite element method was used to numerically solve the liquid film stiffness and damping coefficient under the three degree of freedom perturbation of the end face liquid film, analyzed the influence of different parameters on the dynamic coefficient of liquid film seal, and studied the viscosity wedge effect of the concave surface under the condition of cavitation, and the purpose is to study the pressure distribution and bearing capacity of mechanical seals. Hao et al. (2018) based on the principle of mass conservation, discrete the liquid film control equation by using the finite control volume method, obtained the hydrodynamic performance parameters of the liquid film seal. It was concluded that the values of bearing capacity and friction torque were affected by different surface morphologies, but the effect was limited. Concli et al. (2016) studied the pressure distribution in cavitating small hydrodynamic journal bearings based on the numerical method of the open source CFD program OpenFOAM. Jiang et al. (2019) used ANSYS Fluent to establish a numerical model of three-dimensional flow field of elliptical concave mechanical seal. The research results show that under different direction angles, the location of the proposed geometric convergence point coincides with the maximum pressure point, and the inward flow of the leakage part is the main reason to reduce the leakage rate. Zhang et al. (2022a) based on the mass conservation boundary and the Zwart-Gerber-Belamri cavitation model, carried out numerical calculations on the two forms of rotating mechanical seals and static mechanical seals (slotted on the inner semidiameter side) under different periods and amplitudes. It was concluded that when the pressure disturbance occurred on the outer semidiameter side, the anti-disturbance characteristics of the mechanical seal were significantly enhanced, but it did not consider the dynamic response characteristics of the compensation ring, nor did it affect the single fluctuation Multi wave and alternating loads are studied.

In the study of dynamic characteristics of mechanical seals, Green et al. (1983) calculated the stiffness and damping coefficient of the fluid film in the mechanical face seal for the three main degrees of freedom of the main seal ring. Chen et al. (2017) proposed a new type of dry gas seal with end groove, called super elliptic curve groove, and studied the disturbance behavior of gas film thickness and pressure with and without angular excitation. Blasiak et al. (2016) proposed a gas face seal model, including nonlinear Reynolds equation and dynamic equation describing stator vibration, and solved it simultaneously by numerical method. Sun et al. (2019) analyzed the displacement nonlinear response of the stationary ring based on the non-contact mechanical seal in the frequency domain. According to the harmonic excitation, the output response of the fixed ring is expressed by the famous Volterra series and solved by a new method. This method can be used to analyze the frequency response and calculate the displacement response of the fixed ring under single and double harmonic excitation. Childs et al. (2018) developed a new model for flexible installed stator and flexible installed rotor mechanical seals, including the radial reaction component generated when supporting the O-ring due to the relative extrusion movement on the O-ring. Xu et al. (2020) studied the dynamic contact behavior of liquid lubricated non-contact materials and the transient response of mechanical seals during external pressure fluctuations based on the finite difference method. The mass conservation boundary and the dynamic equation describing stator vibration were used. The results showed that the amplitude and frequency of external pressure vibration had a great impact on the sealing performance. Li et al. (2019, 2020b) established a three degree of freedom dynamic model of mechanical seal based on the finite difference method, and simulated the impact on the mechanical seal through the Gaussian pulse function. In the study, the effects of different amplitudes and angular deviations on the dynamic characteristics of the seal under a single disturbance were discussed. It was found that the fixed angular deviation of the static ring and the initial angular deviation of the dynamic ring had little effect on the axial balance position. When the axial excitation, the film thickness fluctuates sinusoidally from the initial value to the equilibrium position, but its amplitude is much smaller than the excitation amplitude. In addition, the compensation ring will inhibit the occurrence of angular deviation due to the influence of sealing components. Therefore, the axial motion of the compensation ring is mainly considered in the study of the dynamic response characteristics of mechanical seals.

For the mechanical seal used in multiphase pump, the working environment is complex, especially when the multiphase pump encounters extreme working conditions, the stable operation of the mechanical seal directly affects the safety of the pump body. Zhang et al. (2022b) carried out numerical calculation on a self-designed three-stage axial-flow multiphase pump under slug flow condition, and set its inlet as a slug flow condition with an interval between high and low GVF, that is, the GVF changes with time in a rectangular wave, and studied the pressurization capacity of the three-stage pressurization unit in the pump. The change law of the pressurization of the third-stage pressurization unit roughly changes in a triangular function, and the overall fluctuation is more intense. And the difference between the maximum pressurization

and the minimum pressurization is close to 0.1 MPa. When further studying the influence of slug flow on the deformation of pump shaft, the deformation of main shaft changes regularly with time. In addition, Shi et al. (2020) studied the internal pressurization change of multiphase pump, its maximum amplitude was also 0.1 MPa. Therefore, the pressure disturbance waveform studied in this study follows the change of trigonometric function, and the calculation conditions are mostly carried out under the condition that the fluctuation amplitude is 0.1 MPa.

Based on CFD numerical calculation method, this paper establishes the flow field model of spiral groove seal lubrication film, and simplifies it by using periodic boundary conditions. The numerical calculation of cavitation is carried out based on Mixture multiphase flow model and Zwart-Gerber-Belamri cavitation model. On this basis, the fourth-order Runge-Kutta method is used to solve the structural dynamic equation, the weighted average method is used to extract the pressure at the boundary, and the solution process is embedded in the UDF. According to the characteristics of boundary pressure disturbance, the UDF of pressure disturbance wave is compiled. Based on the layered dynamic grid technology, the influence of different amplitude, different period, multi wave interference and other factors on the dynamic response characteristics of mechanical seal under the working condition of pressure disturbance wave at the inlet is studied. The vibration of the shaft system in the pump will produce alternating load, which will affect the stability of the mechanical seal. Based on the original UDF, the function of the alternating load of the spring varying with time is embedded, and the influence of the dynamic response and sealing performance of the compensation ring under the alternating load is studied when the boundary pressure is given. The vibration pattern of the compensation ring and the regulation of the sealing performance of the mechanical seal under the conditions of inlet pressure disturbance and alternating load are explored, and the disturbance mechanism is revealed.

2. Physical model and mesh generation

2.1. Physical model

This study adopts a static mechanical seal (the compensation ring does not rotate with the shaft), and the installation form of the mechanical seal is an internal type. And the research object is the mechanical seal on the side near the multiphase pump in the double end face sealing form, because the mechanical seal here is greatly affected by the pressure fluctuation inside the pump. The mechanical seal structure is shown in Fig. 1, the static ring (compensation ring) is embedded in the pump housing, and only axial vibration occurs. The moving ring is fixed on the pump shaft and rotates with the shaft, and the spiral groove is opened on the moving ring. The pressure of the medium affects the sealing chamber from the multiphase pump side, and then acts on the inner semidiameter side of the sealing ring, while the pressure on the flushing side acts on the outer semidiameter side of the sealing ring.

The geometric model of grooving on the end face of the moving ring is shown in Fig. 2(a), which is divided into groove area, weir area and dam area. The groove profile adopts logarithmic helix, which is shown in Eq. (1). The sealing medium is 4109# lubricating oil, the temperature of the imported lubricating oil is 353 K, the saturated steam pressure is set to 400 Pa, and the diameter of cavitation bubble is 2 μm (Zhang et al., 2022a). The physical parameters of 4109# lubricating oil and oil vapor can refer to Li's article (Li et al., 2015). In order to improve the calculation efficiency, periodic boundary conditions are adopted, and 1/12 of the model is taken as the research object. The layout of measuring points on the sealing end face is shown in Fig. 2(b). Measuring points A and B are located at both ends of the groove root respectively, and measuring point C is located at half the length of the spiral groove. The structural parameters and working conditions parameters of the sealing end face are shown in Table 1.

$$r = r_{\mathrm{in}} \mathrm{e}^{\varphi \tan \theta} \tag{1}$$

In Eq. (1), r_{in} is the inner semidiameter of the sealing ring, mm. φ is the spiral expansion angle, °. θ is the helix angle, °.

2.2. Mesh generation and independence verification

The mesh generation strategy of mechanical seal model is shown in Fig. 3. For convenience of viewing, zoom in 1000 times in the direction of liquid film thickness. The whole model adopts the form of triangular prism mesh, which can well solve the problem that the maximum inclination of the mesh at the sharp corner is too large. The inner semidiameter side is the pressure inlet, the outer semidiameter side is the pressure outlet, and both sides are periodic boundary conditions. The upper end face is the moving ring, and the lower end face is the static ring.

Only consider the axial vibration of the mechanical seal, that is, the number of mesh layers at the film thickness gradually increases or decreases, and more mesh layers will greatly reduce the calculation efficiency. The thickness of lubricating film is about 10~20 μm. The size of the end face is large, and the number of mesh layers is large, which is easy to increase the aspect ratio of the mesh and reduce the quality of the mesh. Therefore, set the mesh size in the film thickness direction to 2 μm. The mesh independence is verified by changing the mesh size of the end face. During mesh independence verification, the film thickness is taken as 15 μm, the inlet pressure is 0.5 MPa, and the outlet pressure is atmospheric pressure. The mesh independence curve is shown in Fig. 4. The fluid force and liquid film cavitation rate gradually decrease with the increase of the number of grids. When the number of grids is about 360000 (that is, the end grid size is 0.115 mm), the fluid force and liquid film cavitation rate basically remain unchanged. Therefore, about 360000 computational grids are selected.

3. Numerical model and verification

3.1. Model assumptions and mathematical models

3.1.1. Model assumptions

In order to reduce the complexity of the study of miscible lubrication film of mechanical seals under pressure fluctuation conditions, factors that have little influence on the calculation are ignored, and the following assumptions are made (Zhang et al., 2022a).

(1) The lubrication film gap is incompressible.
(2) Ignore the influence of seal ring end face roughness.
(3) It is considered that the heat exchange between friction heat and sealing medium has been stable, that is, the temperature of sealing film is constant, which is 353 K.
(4) Ignore the angular deviation caused by the sealing ring, and only consider the axial vibration of the compensation ring.

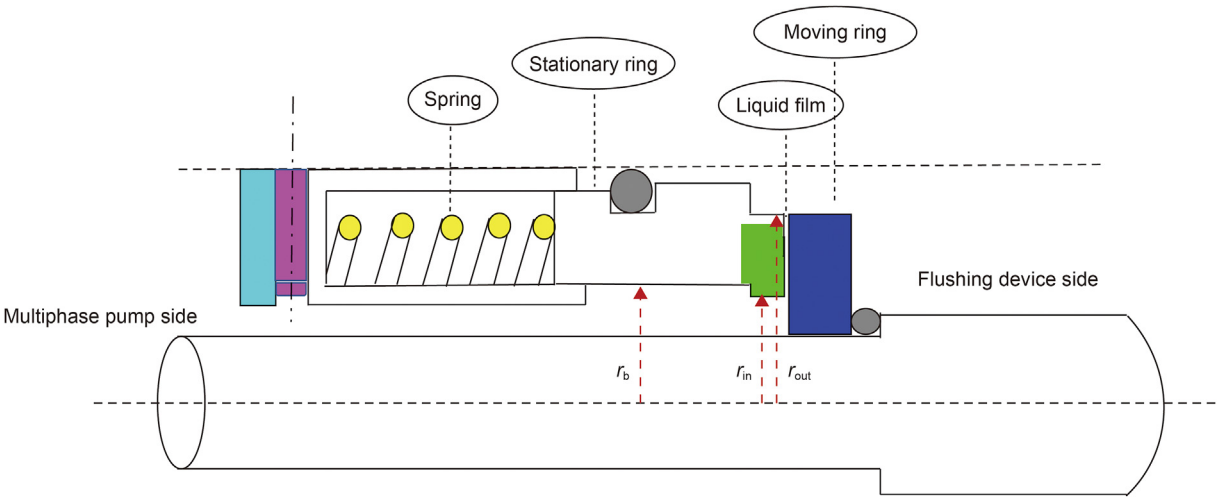

Fig. 1. Schematic diagram of mechanical seal structure.

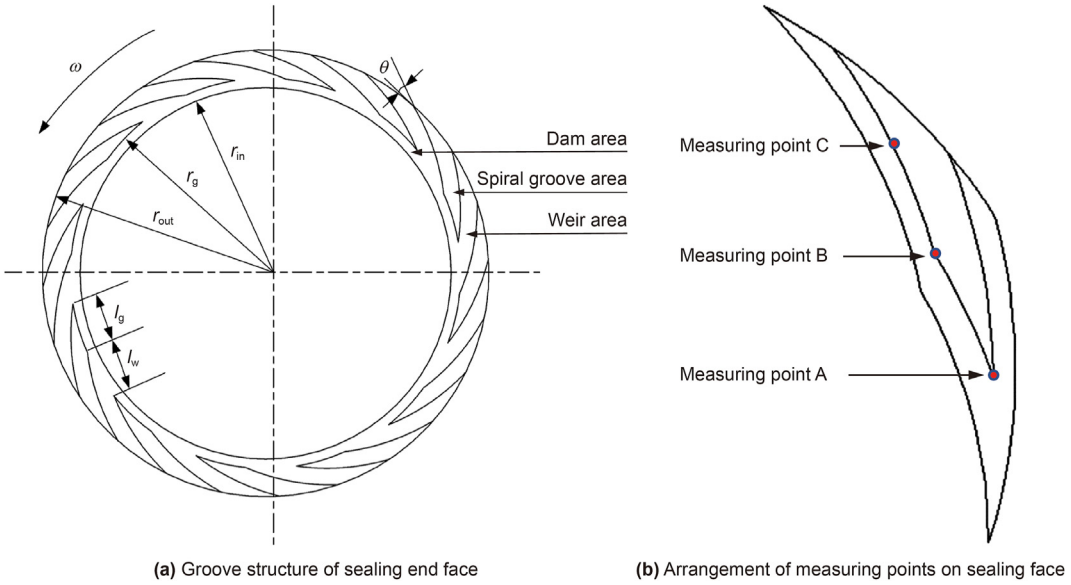

(a) Groove structure of sealing end face **(b)** Arrangement of measuring points on sealing face

Fig. 2. Schematic diagram of groove structure and measuring points of mechanical seal end face.

Table 1
Sealing structure parameters and working condition parameters (Zhang et al., 2022a).

Parameter name	Parameter value
Inner semidiameter of sealing ring r_{in}, mm	44.25
Outer semidiameter of sealing ring r_{out}, mm	53.25
Helix angle θ, °	18
Groove semidiameter ratio β	0.7
Groove width ratio γ	1
Groove depth h_c, μm	8
Number of spiral grooves N	12
Initial film thickness h_0, μm	Determined by calculation
Inlet pressure P_{in}, MPa	UDF
Outlet pressure P_{out}, MPa	0.15
Speed n, rpm	3000

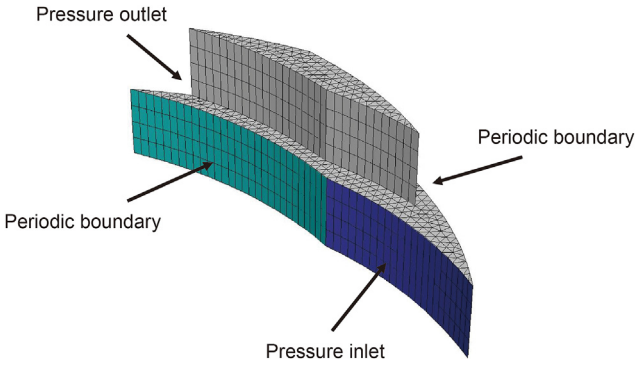

Fig. 3. Mesh generation strategy of liquid film sealing model.

3.1.2. Cavitation model

The cavitation of the sealing gap is caused by the local low pressure at the bottom of the spiral groove, so the Mixture cavitation model is more suitable. Zwart-Gerber-Belamri model is selected, which is closer to the experimental value and has better

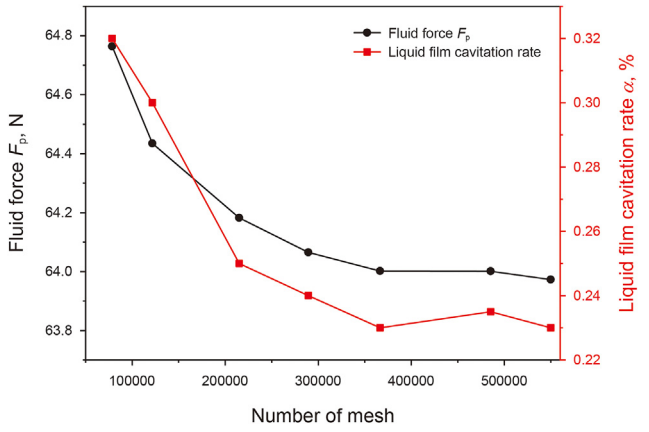

Fig. 4. Verification of mesh independence of liquid film sealing model.

stability (Zhang et al., 2022a).

The continuity equation, momentum equation and gas phase transmission equation based on cavitation (Chen, 2006) are as follows:

$$\frac{\partial \rho_m}{\partial t} + \frac{\partial}{\partial x_i}(\rho_m v_{mi}) = 0 \tag{2}$$

$$\frac{\partial}{\partial x_i}(\rho_m v_{mi}) + v_{mi}\frac{\partial(\rho_m v_{mj})}{\partial x_j} = -\frac{\partial p}{\partial x_i} + \mu_m \frac{\partial}{\partial x_j}\left(\frac{\partial v_{mi}}{\partial x_j} + \frac{\partial v_{mj}}{\partial x_j}\right) \tag{3}$$

$$\frac{\partial}{\partial t}(\alpha\rho_v) + \frac{\partial}{\partial x_i}(\alpha\rho_v v_v) = R_e - R_c \tag{4}$$

In Eqs. (2) and (3):

$$\rho_m = \alpha\rho_v + (1+\alpha)\rho_1 \tag{5}$$

$$\mu_m = \alpha\mu_v + (1-\alpha)\mu_1 \tag{6}$$

Define liquid film cavitation rate α is the ratio of the volume of cavitating gas phase in the sealing film to the volume of the sealing film:

$$\alpha = \frac{V_v}{V_v + V_l} \times 100\% \tag{7}$$

In Eqs. (2)–(7), ρ_m is the mixture density, v_m is the average speed of mass, μ_m is the mixed viscosity coefficient. R_e is the source term for bubble generation, and R_c is the source term for bubble collapse. Subscript v is gas phase and l are liquid phase, α is the cavitation rate of liquid film, V_v is the volume of cavitating vapor, and V_l is the volume of liquid.

According to Chen et al. (2015) and Mayer (1977), the flow inside the mechanical seal is laminar flow. the flow factor ξ is used to determine the flow state of the sealing liquid. When $\xi > 1$, the flow is in a turbulent state, and when $\xi \le 900/1600$, the flow is in a laminar state. The calculation formula is as follows:

$$\xi = \sqrt{\left(\frac{Re_c}{1600}\right)^2 + \left(\frac{Re_p}{900}\right)^2} \tag{8}$$

$$Re_c = \frac{\rho U h}{10^6 \mu} \tag{9}$$

$$Re_p = \frac{\rho v_r h}{10^6 \mu} \tag{10}$$

In the equations, Re_c is the Reynolds number when considering Couette flow alone, Re_p is the Reynolds number when considering Poiseuille flow alone, U is the linear speed of rotation of the end face, m/s. μ is the dynamic viscosity of the liquid film, and v_r is the linear velocity at radius r, m/s.

In order to distinguish the flow state of the liquid between the sealing faces, normal temperature water was taken for analysis. When $n = 10000$ rpm, Re_c was about 0.2. Due to the small leakage in the radial direction, Re_p was much less than 900, resulting in a flow factor $\xi < 900/1600$. The actual operating speed in this article is 3000 rpm, and the viscosity is greater than the viscosity of water, $Re_c < 0.2$, to obtain the flow factor $\xi < 900/1600$ at the actual operating speed, so the actual flow state in the sealed liquid film is laminar flow.

3.1.3. Structural dynamics model

The dynamic model of the liquid film sealing system obtained by properly simplifying the sealing structure is shown in Fig. 5. K and D are the stiffness and damping of the system considering the action of O-ring and spring respectively. The left side is the compensation ring, which can move axially under the action of spring force, the right side is the moving ring, and the spiral groove is opened on the outer semidiameter side of the moving ring. In the structural dynamics equation (Green, 2001), the mass m of the compensation ring is 0.25 kg, the axial stiffness K is 100000 $N \cdot m^{-1}$, the axial damping D is 300 $N \cdot s \cdot m^{-1}$, and the balance ratio is 0.7 (the balance radius r_b can be calculated (Li et al., 2020)).

The dynamic equation of the sealing system is as follows:

$$m\ddot{z}_t + D\dot{z}_t + Kz_t = F_{cls} - F_p = F \tag{11}$$

The closing force equation is as follows:

$$F_{cls} = P_{sp}\pi\left(r_{out}^2 - r_{in}^2\right) + P_{in}\pi\left(r_b^2 - r_{in}^2\right) + P_{out}\pi\left(r_{out}^2 - r_b^2\right) \tag{12}$$

In the equation, π is a constant, and r_b is calculated to be 50.718 mm.

The fluid force equation is as follows:

$$F_p = \int_0^{2\pi}\int_{r_{in}}^{r_{out}} Pr\, dr d\theta \tag{13}$$

Transform Eq. (11) to obtain Eq. (14) as follows:

$$\ddot{z}_t + \frac{D\dot{z}_t}{m} + \frac{Kz_t}{m} = \frac{F}{m} \tag{14}$$

Simplify Eq. (14) and define the natural frequency and damping ratio as follows:

Natural frequency: $\omega_0 = \sqrt{\frac{K}{m}}$.

Damping ratio: $\xi = \frac{D}{2\sqrt{Km}}$.

After simplification, the acceleration of the compensation ring is obtained:

$$\ddot{z}_t = \frac{F}{m} - 2\xi\omega_0\dot{z}_t - \omega_0^2 z_t \tag{15}$$

The fourth-order Runge-Kutta method using high-precision one-step algorithm solves the speed of the compensation loop at time $t + \Delta t$:

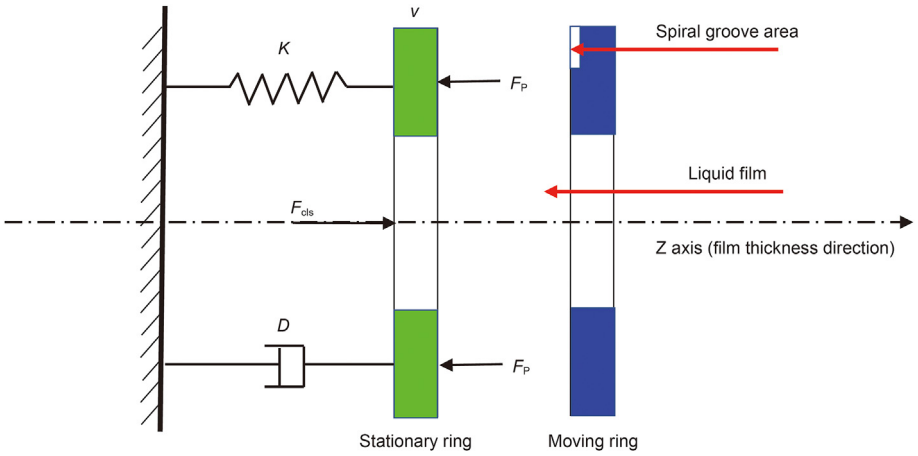

Fig. 5. Dynamic model of sealing structure.

$$k_1 = \frac{F}{m} - 2\xi\omega_0\dot{z}_t - {\omega_0}^2 z_t \tag{16-1}$$

$$k_2 = \frac{F}{m} - 2\xi\omega_0\left(\dot{z}_t + \frac{\Delta t}{2}k_1\right) - {\omega_0}^2\left(z_t + \frac{\Delta t}{2}\dot{z}_t\right) \tag{16-2}$$

$$k_3 = \frac{F}{m} - 2\xi\omega_0\left(\dot{z}_t + \frac{\Delta t}{2}k_2\right) - {\omega_0}^2\left(z_t + \frac{\Delta t}{2}\dot{z}_t + \frac{\Delta t^2}{4}k_1\right) \tag{16-3}$$

$$k_4 = \frac{F}{m} - 2\xi\omega_0(\dot{z}_t + \Delta t \cdot k_3) - {\omega_0}^2\left(z_t + \Delta t \cdot \dot{z}_t + \frac{\Delta t^2}{2}k_2\right) \tag{16-4}$$

$$\dot{z}_{t+\Delta t} = \dot{z}_t + \Delta t \cdot (k_1 + 2k_2 + 2k_3 + k_4)/6 \tag{17}$$

The above solution process is incorporated into UDF. When the pressure fluctuates, F_{cls} in Eq. (9) also changes with time, so it is necessary to extract the pressure at the disturbance boundary. Based on the original UDF, the UDF based on the weighted average method to extract the pressure at the boundary is embedded to realize the change of F_{cls} with time, and finally realize the real-time vibration of the compensation ring when the pressure changes. When the alternating load acts, it is only necessary to embed the function of the alternating load of the spring with time before solving the closed force equation.

3.1.4. Numerical method and calculation process

Coupled algorithm is used in numerical calculation, Green-Gauss Cell Based is used for gradient space discretization, and PRESTO! format is used for pressure term, first-order upwind format is used for volume fraction term, and second-order upwind format is used for others. The fourth-order Runge-Kutta method is used to solve the velocity of the compensation ring in the structural dynamic equation, the weighted average method is used to extract the pressure at the inlet boundary, and the layered dynamic mesh technology is used for mesh updating. The technical route of liquid film seal dynamics research based on fluid-structure interaction (FSI) theory is shown in Fig. 6.

3.2. Feasibility verification of numerical methods

Based on the experimental data (Yang, 2019), the correctness of the numerical calculation method in this study is verified, and the structural parameters of the verified model are shown in Table 2.

The cavitation of the seal end face in the experiment is shown in Fig. 7(a). With the increase of the speed, the cavitation area of the end face increases significantly. When the speed is less than 1000 rpm, the cavitation area in the experiment basically disappears. The end face cavitation results at equilibrium calculated based on the numerical calculation method in this study are shown in Fig. 7(b). The change trend of the cavitation cloud diagram is consistent with the experimental trend, and the size of the cavitation area is also similar. There is a weak cavitation area at 1000 rpm, However, its proportion is extremely small and negligible. It can be seen from Fig. 7 that the numerical calculation method in this study has high calculation accuracy for the cavitation of mechanical seal end face.

Further verify the balance film thickness h_b, as shown in Fig. 8. The numerical calculation results of the smooth seal face are consistent with the balance film thickness trend obtained from the experiment under the rough end face, but there is a certain difference between the two film thicknesses. The reasons for the difference are as follows: (1) the laminar flow model cannot consider the wall roughness. (2) The effect of rough peak bearing capacity is not considered for the smooth sealing face.

The result of numerical calculation of end face smoothness in Fig. 8 is smaller than the experimental value, because when considering the rough surface, it is necessary to increase the rough peak bearing capacity F_{as} in Eq. (11), as shown in Eq. (18), F_{as} and F_p are in the same direction, which has a promoting significance for increasing the film thickness. Therefore, under the same closing force, the end face smoothness is smaller than the balance film thickness calculated by end face roughness, but the value of F_{as} is smaller, which has little change to the film thickness of mechanical seal.

$$m\ddot{z}_t + D\dot{z}_t + Kz_t = F_{cls} - F_p - F_{as} \tag{18}$$

In the equation, F_{as} is the rough peak bearing capacity.

The overall trend of the numerical results is consistent with the experimental results, and the difference of the balance film thickness between the two is small, which further explains the reliability and correctness of the numerical calculation of the smooth plane. Therefore, this study uses smooth walls for numerical calculations.

3.3. Boundary condition setting and initial film thickness calculation (h_0)

Based on the control variable method, the effects of inlet

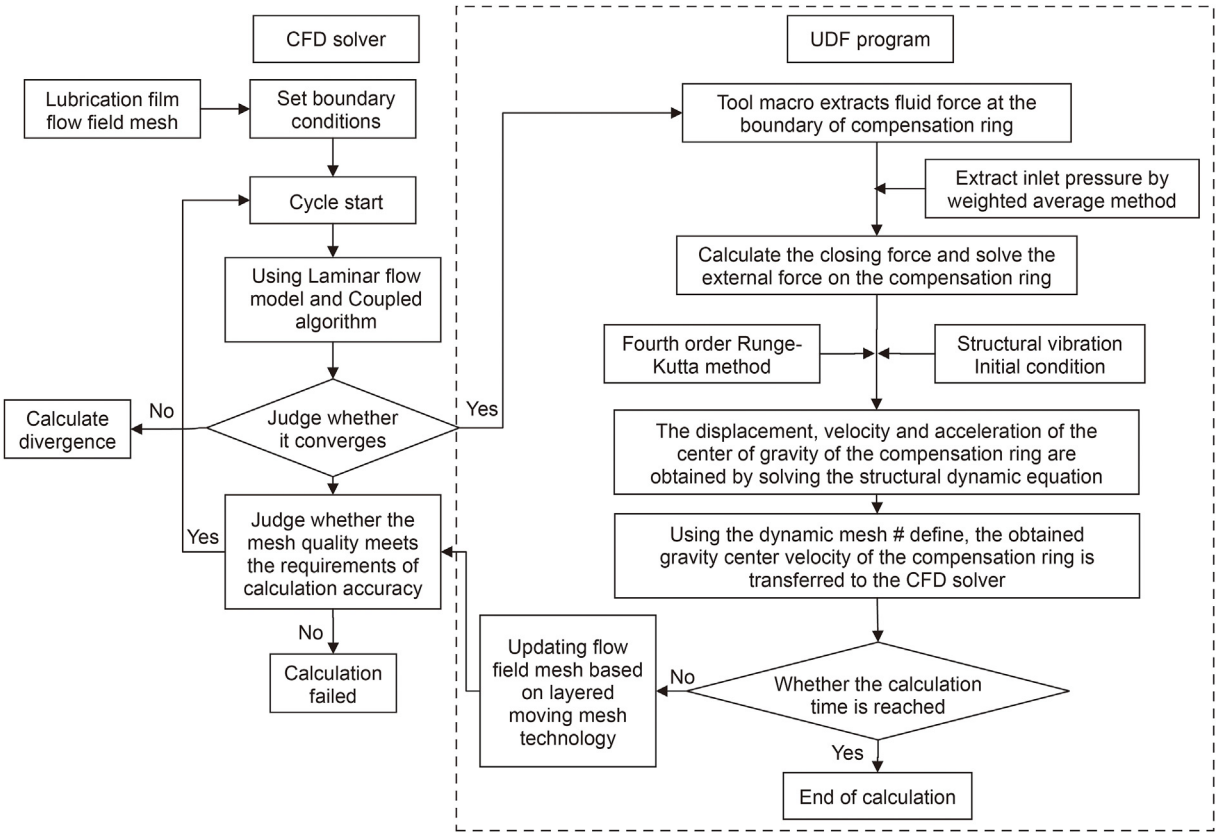

Fig. 6. Technical route of liquid film sealing dynamics research based on FSI theory.

Table 2
Structural parameters of validation model.

Structural parameters	Internal semidiameter r_{in}, mm	External semidiameter r_{out}, mm	Spiral groove radius r_g, mm	Groove depth h_c, μm	Helix angle θ, °	Number of spiral grooves N
Value	46.25	55.25	52.55	12	27	12

pressure disturbance and alternating load on the dynamic response of mechanical seals are studied, that is, when the pressure disturbance, the alternating load is a fixed value. When the alternating load changes, the boundary pressure is a constant value.

In this study, considering that the inlet (inner semidiameter side) pressure boundary is disturbed, and the outlet (outer semidiameter side) pressure is a fixed value, according to the introduction, the set pressure disturbance follows the trigonometric function change, and the equation is as follows:

$$P_{in} = \begin{cases} -P_0 \cdot \cos(\omega \Delta t) + P_0 + P_1, & \text{Disturbance period} \\ P_1, & \text{Stable period} \end{cases} \quad (19)$$

In the equation, P_1 is the initial inlet pressure, P_0 is half of the fluctuation amplitude, ω is the angular frequency, Δt is the difference between the current calculation time and the corresponding time at the initial time of disturbance (0.045 s is taken as the initial disturbance time in this study).

During the actual operation of the mechanical seal, the change of the load on the spring is very complex, and it is difficult to extract the specific expression of the spring alternating load P_{spt}. Therefore, the paper adopts the spring alternating load function mentioned in the literature (Sun et al., 2017), that is, the sine function, and the equation is as follows:

$$P_{spt} = \begin{cases} C_1 \cdot 150000 \cdot \sin(\omega \Delta t) + 150000(\text{Pa}), & \text{Disturbance period} \\ 150000(\text{Pa}), & \text{Stable period} \end{cases} \quad (20)$$

In the equation, P_{spt} is the alternating load of the spring, that is, the specific pressure of the spring changes with time, C_1 is a constant, which is used to change the amplitude of Eq. (20), and angular frequency ω calculate the disturbance period (an alternating period is taken in this study).

For mechanical seals for pumps, when the working pressure is below 2 MPa, the flushing pressure is 0.05–0.2 MPa greater than the pressure in the seal chamber. Therefore, in this study, the flushing pressure is 0.15 MPa, that is, the outlet pressure P_{out}. The inlet pressure is 0.1 MPa, that is, the pressure in the seal chamber (Zhang et al., 2022a). When there is no pressure fluctuation, the fluid flow direction is from the outer diameter side to the inner diameter side for leakage. When pressure fluctuations occur, the pressure on the inner diameter side is higher than the pressure on the outer diameter side, regardless of the influence of the rotating

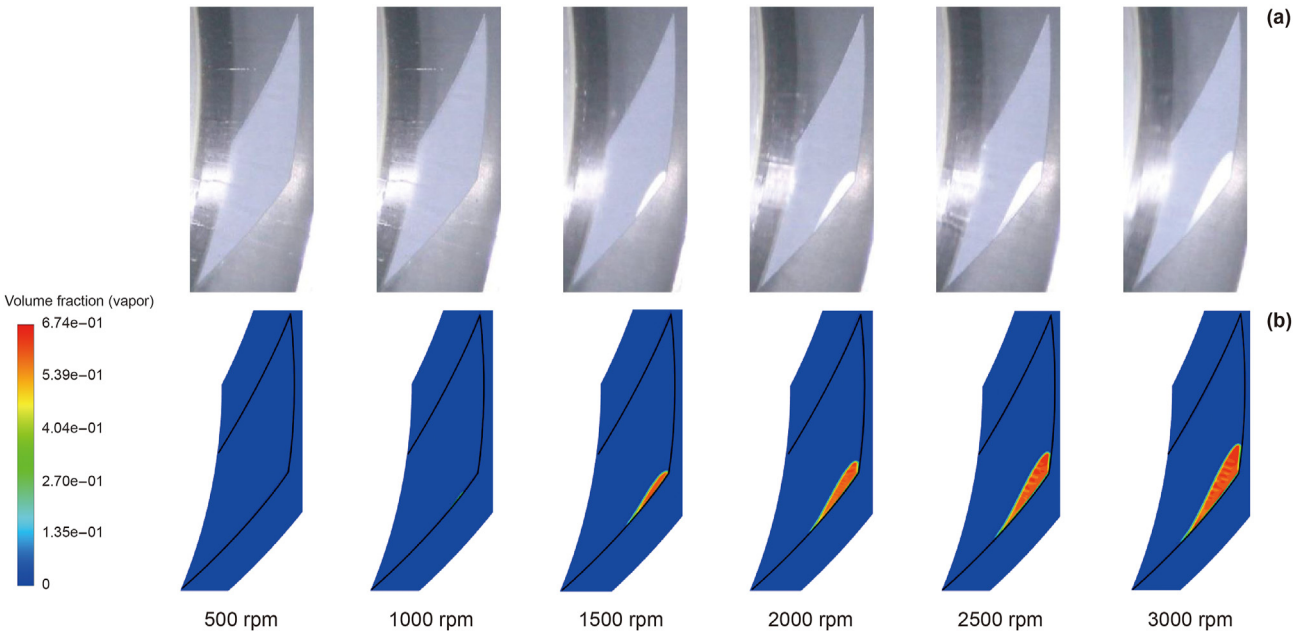

Fig. 7. End face cavitation diagram at balance.

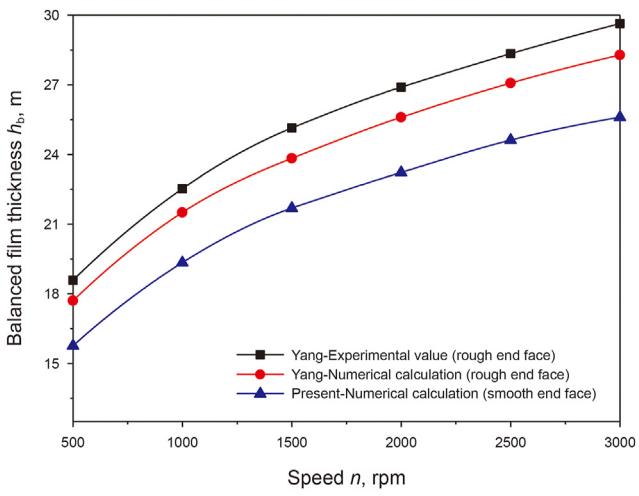

Fig. 8. Calculation and verification of balance film thickness h_b.

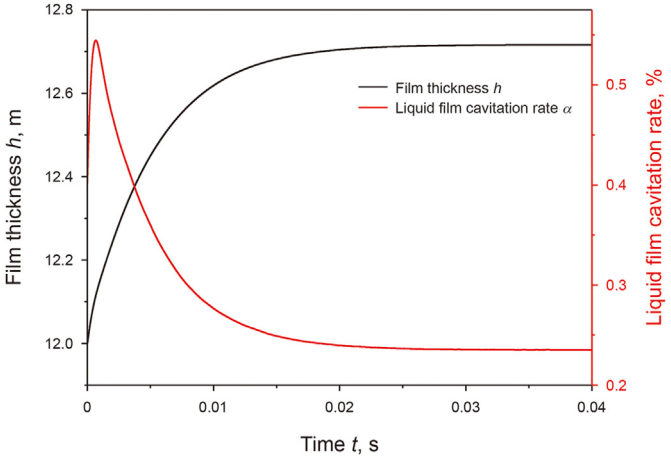

Fig. 9. Variation of film thickness and liquid film cavitation rate with time.

ring. At this time, the fluid flow direction is leakage on the inner diameter side and outer diameter side. The same mesh size is used to calculate the initial film thickness, the time step is 0.000002 s, and the spring specific pressure P_{sp} at the initial time is 0.15 MPa. The calculation results are shown in Table 3.

According to the boundary conditions and structural parameters, the closing force of the compensation ring is 60.878 N. In view of the dynamic mesh characteristics of the layered mesh, that is, the mesh changes by more than 2 μm, the number of mesh layers increases or decreases correspondingly, and the initial film thickness h_0 is taken as 12 μm.

Table 3
Calculation of initial film thickness.

Assumed film thickness h_a, μm	15	12	10
Fluid force F_p, N	47.947	66.15	89.291

3.4. Calculation of balance film thickness (h_b)

When considering the influence of inlet pressure disturbance or spring alternating load on mechanical seal, it is necessary to first determine the balance film thickness of mechanical seal compensation ring under stable boundary conditions, and apply inlet boundary pressure disturbance or spring alternating load based on the balance film thickness. Based on the numerical calculation method in this study, the balance film thickness calculation is carried out. The variation of film thickness and liquid film cavitation rate with time is shown in Fig. 9. At 0.04 s, the film thickness has basically remained unchanged with time, that is, the balance film thickness. When the compensation ring is stable, the obtained balance film thickness h_b, fluid force F_p, and liquid film cavitation rate α and leakage Q are shown in Table 4.

When the film thickness is balanced, the cavitation and pressure distribution of the mechanical seal end face are respectively shown in Fig. 10(a) and (b). The cavitation area of the seal end face in Fig. 10(a) is small and distributed on the left side of the groove. In

Table 4
Calculation of balanced film thickness.

	Balanced film thickness h_b, μm	Fluid force F_p, N	Liquid film cavitation rate A, %	Leakage volume Q, 10^{-6} kg·s^{-1})
UDF	12.71643	60.302	0. 235	75.35

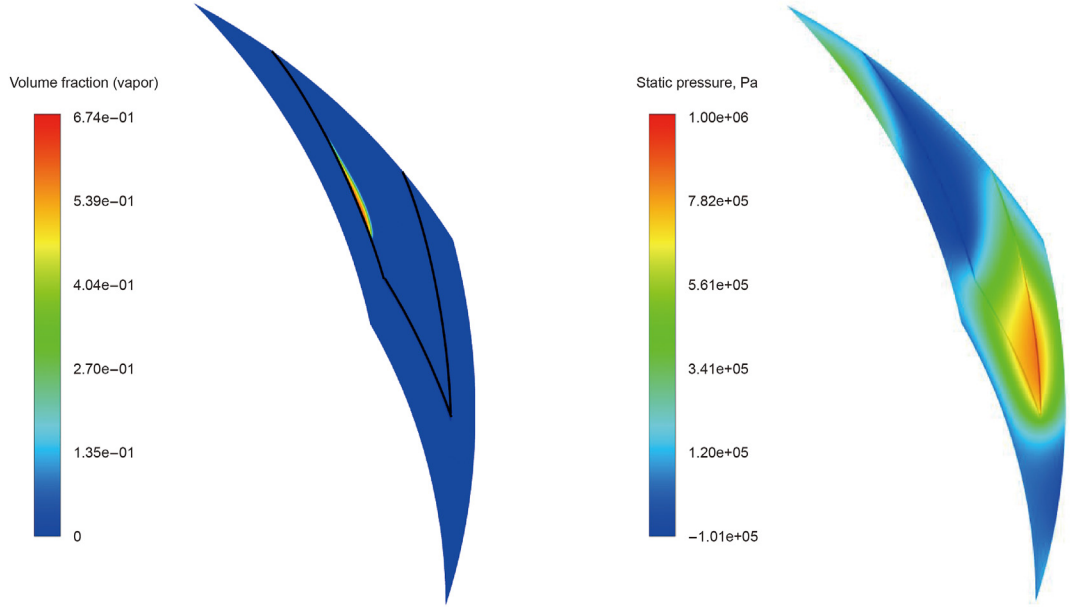

(a) Sealing face cavitation cloud diagram **(b)** Pressure distribution of sealing face

Fig. 10. Calculation and verification of balance film thickness h_b.

Fig. 10(b), the high-pressure area mainly exists at the top of the spiral groove, and the maximum pressure is 1 MPa. The cavitation area is mainly caused by the local pressure on the end face being lower than the saturated steam pressure. From the perspective of the structure of mechanical seals, the cavitation mechanism of mechanical seals is explained. Due to the counterclockwise rotation, the working medium has successively experienced backstage step flow and forward step flow. It should be noted that the studied sealing liquid film thickness is about 12 μm, belonging to the micrometer level. Therefore, a pressure drop will occur at the backstage step. When it is below the saturated vapor pressure, the working medium undergoes cavitation. Due to the obstruction of the front steps, a high-pressure area will appear at the top of the spiral groove.

4. Results and analysis

Based on the FSI theory, the dynamic response characteristics of liquid film seal are studied. The vibration of the compensation ring is realized by embedding UDF and dynamic mesh technology, and the influence of pressure disturbance amplitude, period and multi wave disturbance at the inlet of the seal ring on the mechanical seal is further explored. Considering the influence of the spring alternating load caused by the pressure disturbance wave, the dynamic response characteristics of the spring alternating load acting on the back side of the compensation ring of the mechanical seal are studied under the stable boundary pressure condition. Based on the research results, the effects of pressure disturbance wave and spring alternating load on the vibration characteristics and sealing performance of the compensation ring are comprehensively compared.

4.1. Influence of inlet pressure disturbance wave on compensation ring

4.1.1. Influence of disturbance amplitude on compensation loop

The amplitude of pressure disturbance is the main factor affecting the vibration of mechanical seals. In this study, the commercial software Fluent is used to study the working condition of small disturbance amplitude. Embed the boundary condition function into UDF, that is, Eq. (16), and then change the amplitude of pressure fluctuation by changing P_0. The change of inlet pressure is shown in Fig. 11(a). Set the difference between disturbance amplitudes as 0.05 MPa, the period from 0.04 to 0.045 s is considered as the early stage of disturbance (balance period), providing a stable operating environment for mechanical sealing. The period from 0.045 to 0.055 s is considered as the pressure disturbance period, and the pressure disturbance follows the change of trigonometric function. The period from 0.055 to 0.08 s is considered as the pressure stability period, and provide time guarantee for the recovery and stability of the compensation ring.

The variation of fluid force with time is shown in Fig. 11(b), and its trend is consistent with the trend of inlet pressure, which corresponds to the beginning and end time of pressure disturbance one by one. When the inlet pressure fluctuates, the flow force and closing force are always balanced in the numerical calculation process, which is basically consistent with the results of Li et al. (2020b), mainly because the wall surface is smooth in the numerical calculation, and the wall roughness is not considered, so there is no rough peak bearing capacity in the structural dynamics equation. In addition, the film thickness of the lubricating film of mechanical seals is in the micron scale, and the difference between the end face size and the film thickness is 10^{-5}, and the fluid force is

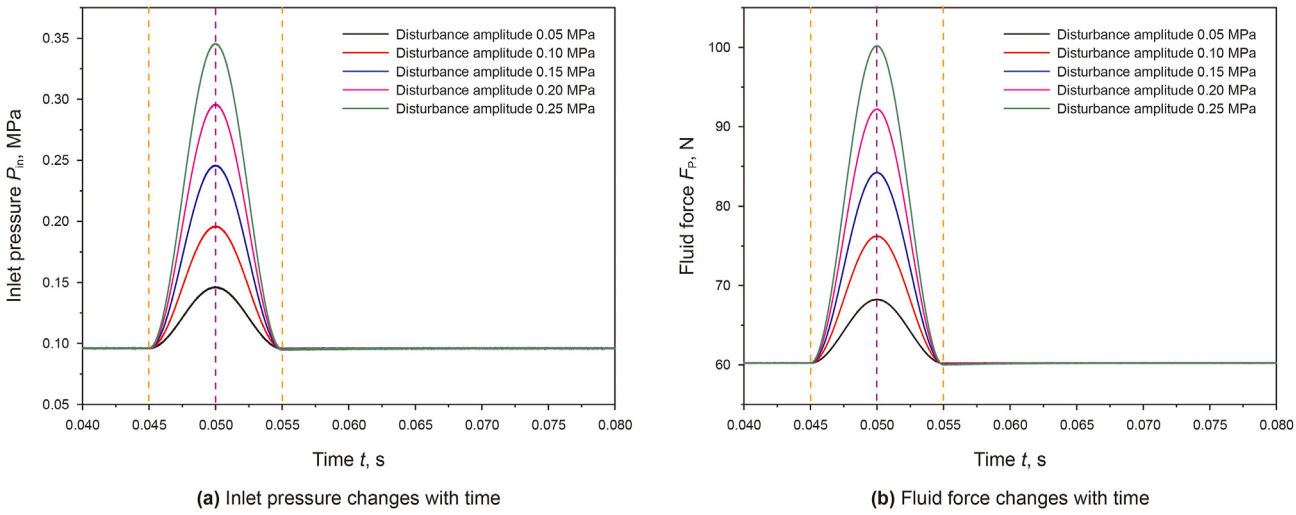

(a) Inlet pressure changes with time **(b)** Fluid force changes with time

Fig. 11. Change of inlet pressure and fluid force with time.

far greater than the contact force. Therefore, the instantaneous fluctuation of fluid force is basically synchronized with the pressure disturbance, and the value is basically consistent with the closing force. In the subsequent research, the fluid force and the closing force are always balanced.

Further study the vibration characteristics of the compensation ring. As shown in Fig. 12(a), the film thickness change curve is divided into: pre disturbance period, disturbance period, disturbance recovery period and equilibrium period. As the disturbance time goes on, the thickness of lubricating film decreases first and then increases. There is vibration lag from 0.045 s to the motion of the compensation ring, but the lag time is extremely small, and gradually decreases with the increase of disturbance amplitude. At 0.052 s, the film thickness changes to the minimum value, and with the increase of disturbance amplitude, the film thickness gradually decreases, and the variation amplitude is basically the same. There is a phase difference between the minimum film thickness and the peak value of pressure disturbance, and the phase difference is independent of the amplitude of pressure disturbance. At 0.066–0.08 s, the change of film thickness tends to be stable, and the local enlarged figure is shown in Fig. 12(b). Taking the balance film thickness calculated by UDF as the benchmark, with the increase of disturbance amplitude, the time required for the film thickness to recover smoothly gradually increases, and the difference of disturbance recovery time gradually decreases.

After the pressure disturbance, the film thickness has not yet recovered to the balance film thickness, mainly due to the damping effect of the liquid film. At this time, the pressure field in the lubricating film has not yet fully recovered (Li et al., 2020b). In addition, according to the pressure at measurement points, as shown in Fig. 13, at the end of the pressure disturbance, the pressure at measurement point C has recovered in advance, while the pressure at measurement points A and B has not recovered. Measuring points A and B are at the groove root, and the groove root radius is in the high-pressure area due to the influence of the spiral groove pumping effect. Therefore, the incomplete pressure recovery in the high-pressure region is the main reason for the disturbed recovery period of the film thickness change curve.

When the pressure disturbance wave acts, the cavitation rate of the liquid film changes with time, as shown in Fig. 14(a). Due to the pressure disturbance at the inlet, the compensation ring moves back and forth. When the film thickness decreases, the

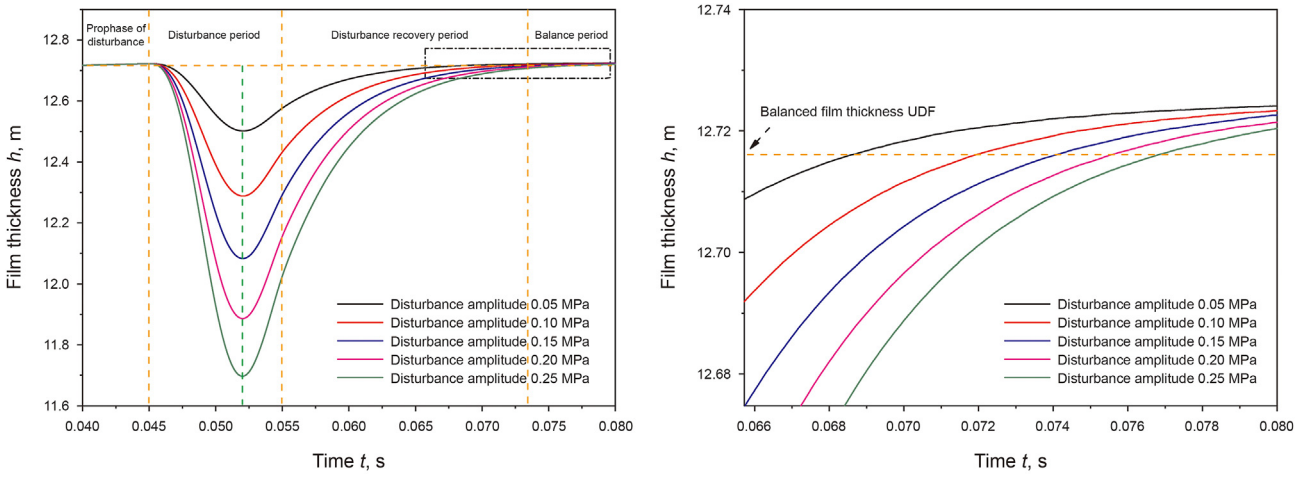

(a) Film thickness change **(b)** Partial enlarged view of film thickness change

Fig. 12. Film thickness changes with time.

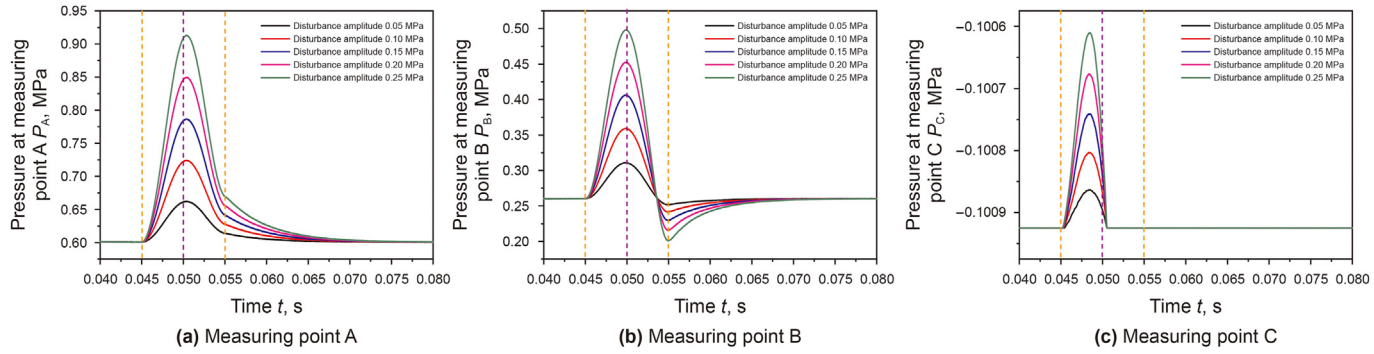

Fig. 13. Variation of pressure film thickness at measuring points with time.

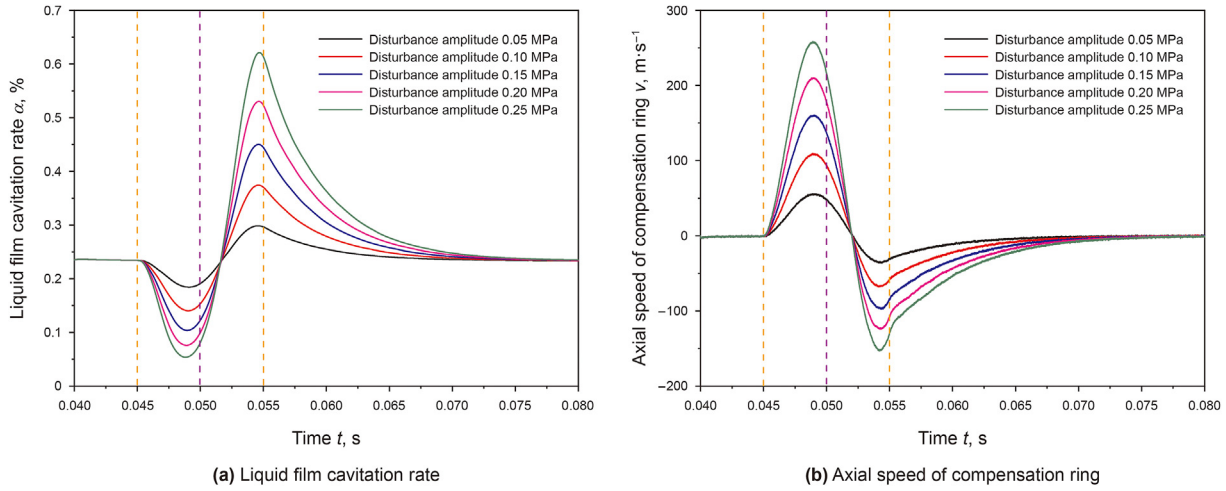

Fig. 14. Variation of liquid film cavitation rate and axial velocity of compensation ring with time.

compensation ring squeezes the liquid film, and the internal pressure gradually increases, resulting in the reduction of the low-pressure area, and the gas generated by cavitation in the liquid film gradually decreases. When the film thickness is reduced to the minimum value, the volume of gas phase in the liquid film due to cavitation gradually increases to the initial value. When the film thickness recovers from the minimum value to the balance film thickness, the liquid film cavitation rate increases first and then decreases. At about 0.055 s, the liquid film cavitation rate is the largest, and the maximum value is about 0.623%. The hysteresis between the liquid film cavitation rate and the pressure disturbance is also caused by the damping effect of the liquid film, which makes the pressure in the high-pressure area unable to recover in time. The variation of axial speed of compensation ring with time is shown in Fig. 14(b). The variation of axial speed approximately follows the cosine function, and the maximum axial speed is about 259.7 μm/s, the maximum displacement corresponding to the unit time step is 0.0005194 μm. In addition, comparing Fig. 14(a) and (b), the change speed of the liquid film cavitation rate is determined by the axial speed, and the amplitude of the two is negatively correlated, that is, when the axial speed is at the peak, the liquid film cavitation rate is at the minimum. The phase difference between the two curves is π, that is, it changes inversely with time.

The pressure disturbance causes the compensation ring to move, which is bound to cause the leakage volume to change. As shown in Fig. 15, the leakage volume changes with time. With the increase of disturbance amplitude, the increase of leakage volume gradually increases. The minimum value of leakage volume is about

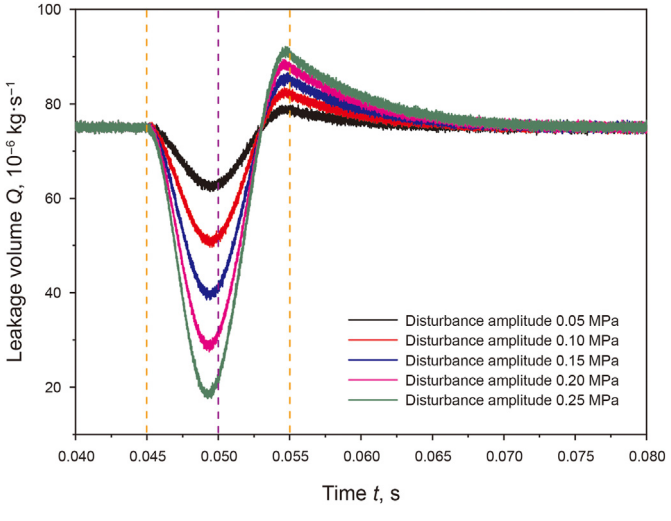

Fig. 15. Change of leakage with time.

18.06 mg/s, and the corresponding time is about 0.049 s. At this time, the pressure at measuring points A and B is also at the peak, indicating that the increase of pressure at the groove root radius can significantly improve the leakage volume. At 0.055 s, the pressure disturbance ends and the leakage increases to the peak, but the increment is far less than the corresponding leakage change

value at 0.049 s. In addition, the leakage also has hysteresis.

4.1.2. Influence of disturbance period on compensation loop

The disturbance period directly affects the closing force and the time of fluid force acting on the compensation ring, which can effectively reduce the hysteresis of various parameters of mechanical seal caused by pressure disturbance. Set the pressure disturbance amplitude to 0.1 MPa by changing the angular frequency ω to change the disturbance period. The change of inlet pressure with time is shown in Fig. 16. Considering the calculation time and efficiency, the difference between the disturbance periods is set to be 0.0025 s.

Affected by the disturbance period, the film thickness of the lubrication film changes with time, as shown in Fig. 17(a). With the increase of the disturbance period, the film thickness gradually decreases, and the time required for the disturbance recovery period gradually increases. The minimum film thickness moves to the left with the increase of the disturbance period, and the minimum film thickness is 12.20 μm. The variation of the liquid film cavitation rate with time is shown in Fig. 17(b). In the stage of decreasing the liquid film cavitation rate, the increment of the liquid film cavitation rate gradually decreases with the increase of the disturbance period, while in the stage of increasing the liquid film cavitation rate, the liquid film cavitation rate increases with the increase of the disturbance period. At the end of the disturbance, except for the disturbance period of 0.005 and 0.0075 s, the liquid film cavitation rate under other working conditions began to decrease before the end of the disturbance, and with the increase of the disturbance period, the advance time gradually increased. The pressure at the measuring point changes with time, as shown in Fig. 18. The pressure peak at measuring point A gradually increases with the increase of disturbance period. In the process of disturbance, the pressure at measuring point A is always above the initial pressure, which is consistent with that at measuring point C, but the peak value of pressure at measuring point C gradually decreases with the increase of disturbance period. The pressure at measuring point B is less than the initial pressure for a certain period, but its minimum and maximum values are basically independent of the disturbance period. At the end of the pressure disturbance, the pressure at measuring point C has been restored, while the pressure at measuring points A and B has not been restored. Comparing the pressure at measuring points A and B at the end time, the pressure at measuring point A is greater than that at measuring point B. Therefore, the pressure at measuring point A is the fundamental reason why the pressure on the lubricating film end face has not been restored in time.

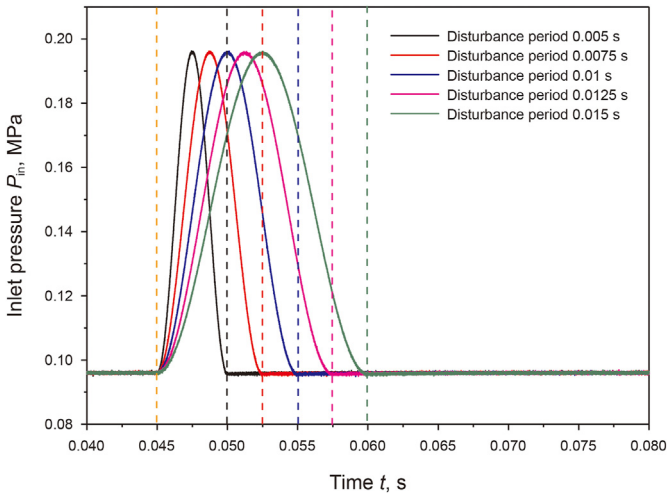

Fig. 16. Pressure change at inlet with time.

Further study the axial speed of the compensation ring and the leakage of the mechanical seal, as shown in Fig. 19(a) and (b), respectively. During the increase period of the axial speed, the peak value of the axial speed gradually decreases with the increase of the disturbance period. When the axial velocity decreases, the minimum value of the axial velocity is independent of the disturbance period. The change trend of leakage is opposite to the axial speed. In the stage of decreasing leakage, the increment of leakage gradually decreases with the increase of disturbance period. The minimum value of leakage is about 45 mg/s, which occurs when the disturbance period is 0.005 s. In the rising stage, the peak value of leakage is basically the same.

4.1.3. Influence of multi disturbance wave on compensation loop

The single wave disturbance condition has been discussed above, and the vibration characteristics of multi wave disturbance on the mechanical seal compensation ring need to be further explored. Set the disturbance period of 0.01 s and the disturbance amplitude of 0.1 MPa, and carry out numerical calculation. The long-term pressure disturbance condition can be decomposed into stable pressure disturbance wave (stable wave), gradually increasing pressure disturbance wave (enhanced wave) and gradually decreasing pressure disturbance wave (attenuation wave). By analyzing the mutual interference law between fluctuations, the dynamic response characteristics and sealing performance changes of mechanical seal compensation ring under the long-term pressure disturbance condition can be further predicted. Considering the superposition and consumption of fluctuations, set the amplitude change of enhancement wave (or attenuation wave) to be 2 times (or half) of the amplitude value of the previous pressure disturbance, and the disturbance period remains unchanged.

As shown in Fig. 20(a), (b) and (c) are the corresponding parameter change curves under the conditions of stable disturbance, enhanced wave, and attenuated wave respectively. In Fig. 20(a), the stable disturbance wave promotes the reduction of film thickness, but the increment of film thickness is gradually decreasing. In the disturbance period, the first wave makes the film thickness gradually reduce, and the second and third waves maintain the compensation ring to vibrate slightly at the position of small film thickness. In Fig. 20(b), with the increase of disturbance amplitude, the film thickness increment gradually increases. When the pressure disturbance amplitude is 0.1 MPa, the film thickness reaches the minimum value, which is basically consistent with the film thickness corresponding to a single disturbance wave, indicating that the influence of enhanced wave interference on the film thickness is not obvious in a small pressure disturbance range, because the increase of fluctuation amplitude provides more fluid kinetic energy for the compensation ring. In order to maintain balance, The compensation ring continues to vibrate, and the flow force and closing force are determined by the inlet pressure. In Fig. 20(c), as the disturbance amplitude decreases, the film thickness increment gradually decreases. The first wave is consistent with the pressure disturbance amplitude of 0.1 MPa, but it has an impact on the film thickness of the latter two fluctuation times, that is, the film thickness in the attenuation wave is smaller than that in Fig. 20(b). The cavitation rate of the liquid film in the lubricating film is further studied. When the pressure fluctuation is stable, the peak value of the cavitation rate of the liquid film increases wave by wave, while the axial velocity of the compensation ring decreases gradually with the fluctuation. In the influence of enhancement wave and attenuation wave on the liquid film cavitation rate and axial velocity, it is found that the liquid film cavitation rate and axial

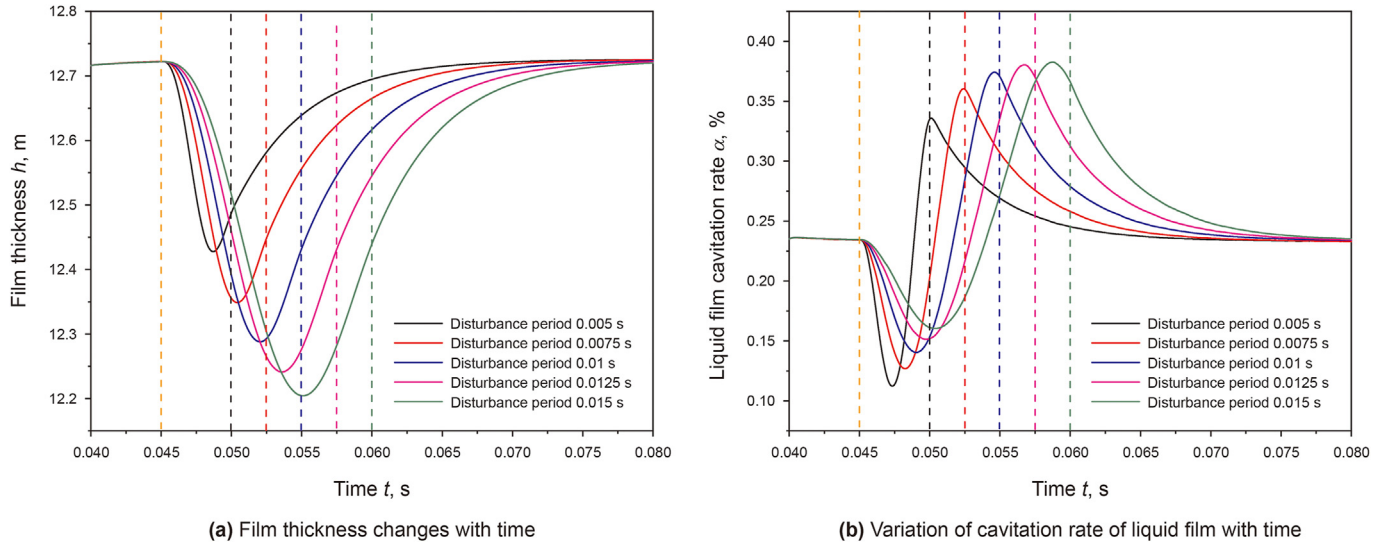

Fig. 17. Variation of film thickness and liquid film cavitation rate with time.

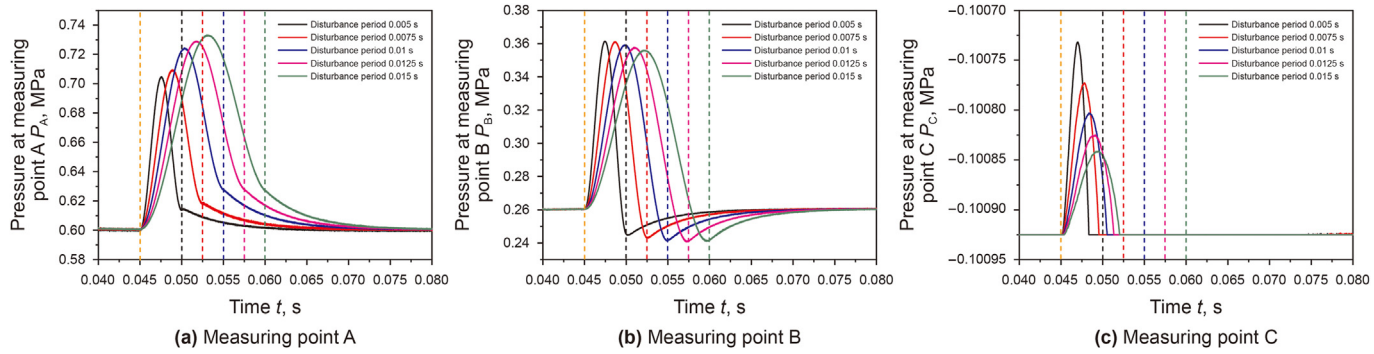

Fig. 18. Pressure change of measuring points with time.

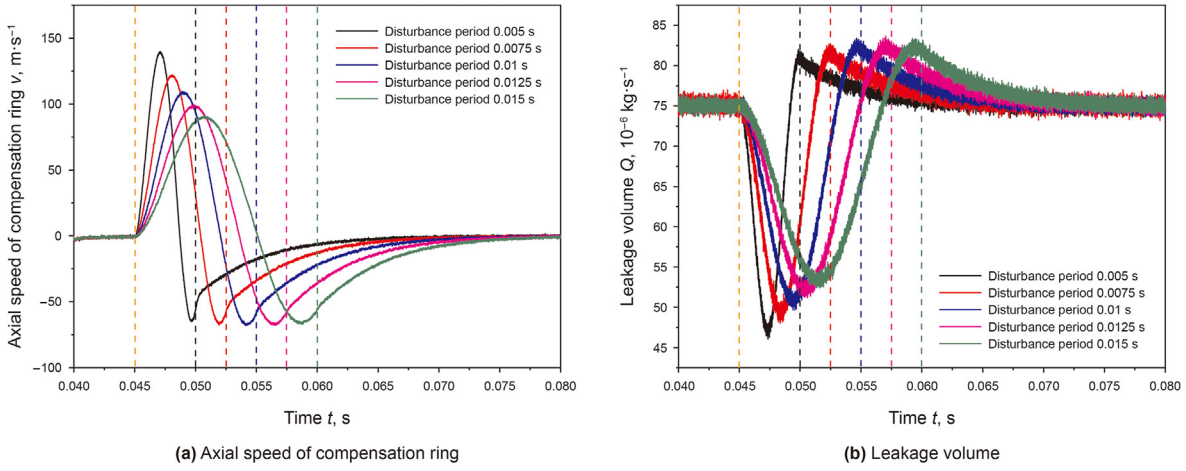

Fig. 19. Variation of axial speed and leakage of compensation ring with time.

velocity fluctuate near the initial value when the mechanical seal is in the condition of enhancement wave, while under the condition of attenuation wave, the fluctuation of liquid film cavitation rate is above the initial value, and the fluctuation of axial velocity is below the initial value.

As shown in Fig. 21(a), (b) and (c), the corresponding leakage volume and pressure change curve of the measuring point under the stable disturbance, enhanced wave and attenuated wave conditions are respectively. Under the stable disturbance condition, the leakage volume fluctuates below the initial value, and this phenomenon occurs under the enhanced wave and attenuated wave conditions, indicating that a small increase in inlet pressure under

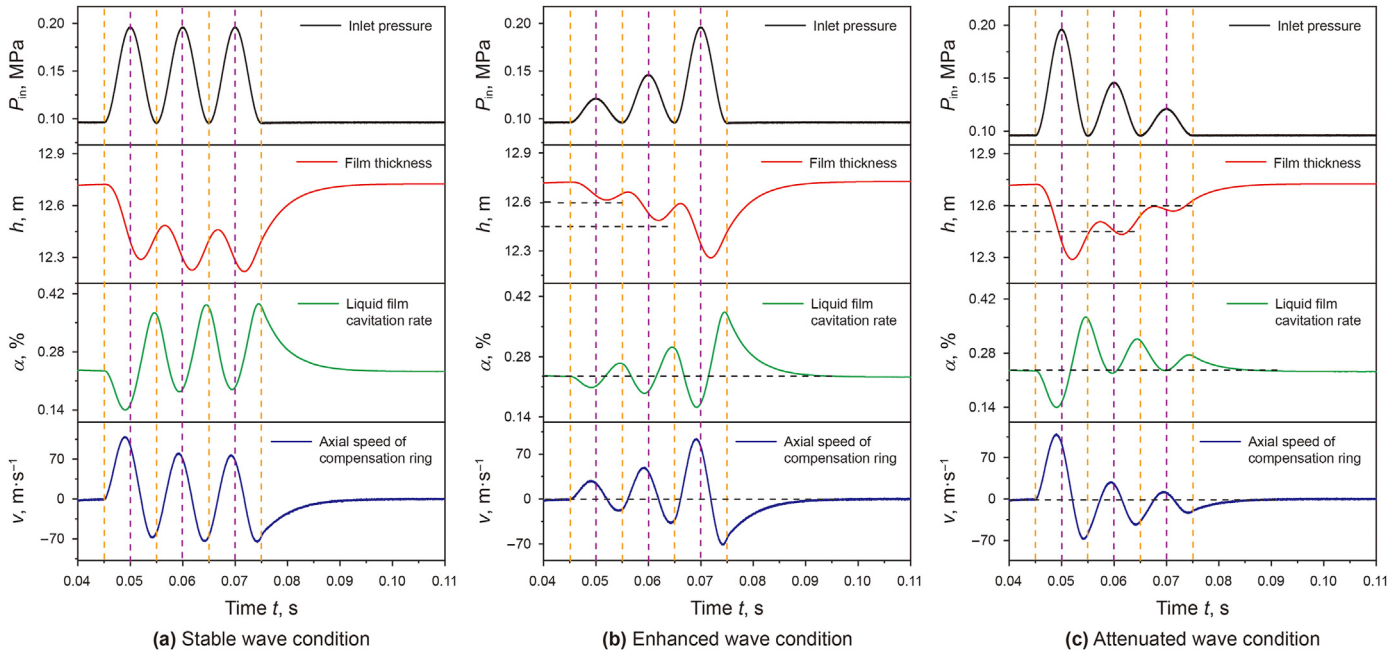

Fig. 20. Variation of inlet pressure, film thickness, liquid film cavitation rate and axial velocity with time under multi wave disturbance condition.

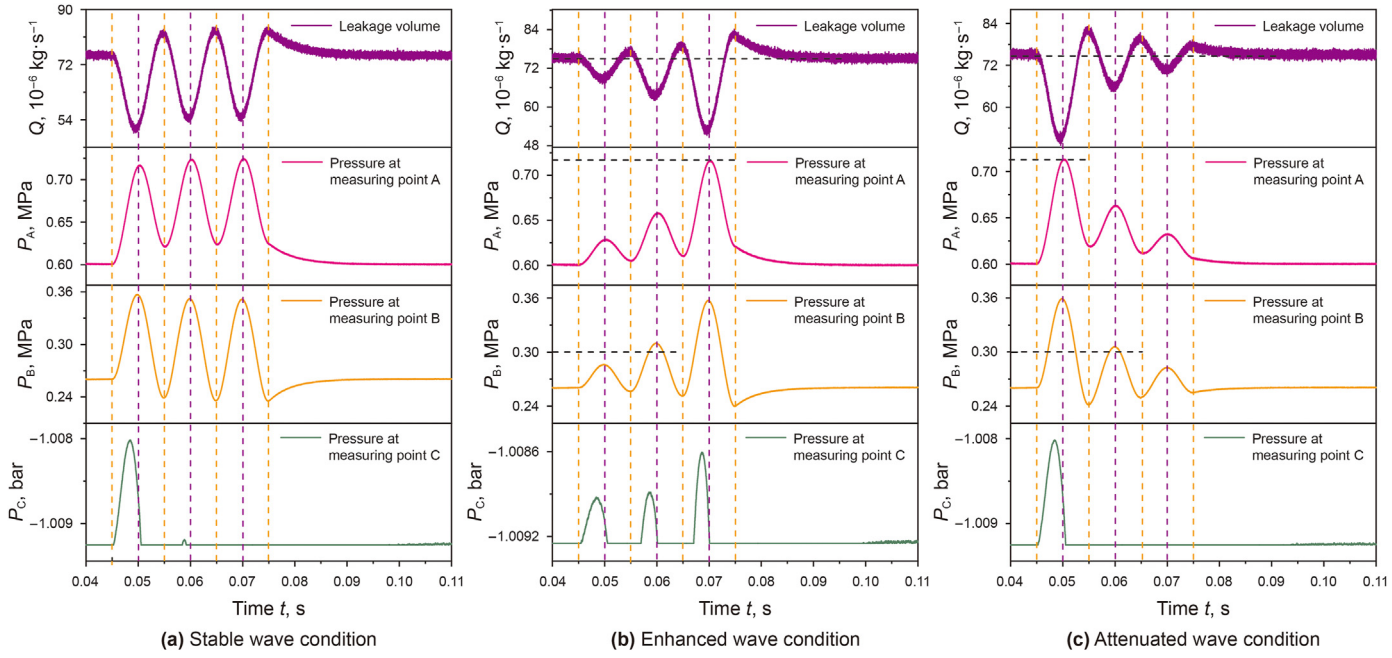

Fig. 21. Variation of leakage and pressure at measuring point with time under multi wave disturbance conditions.

this operating condition is helpful to reduce leakage. Compared with the attenuation wave, the leakage of the latter deviates more from the initial value. The deviation phenomenon under multiple disturbance waves can be explained by the change of end pressure. The end pressure is mainly in the high-pressure area. The peak value of pressure at measuring points A and B under the enhanced wave condition is slightly higher than that under the attenuation condition, while the increase of pressure in the lubricating film, especially at the groove root, helps to reduce the leakage. Higher pressure can lead to smaller cavitation rate and larger film thickness.

4.2. Influence of spring alternating load on compensation ring

4.2.1. Influence of load amplitude on compensation ring

During the actual operation of the multiphase pump, the load on the spring is difficult to measure, so the setting of the spring alternating load as a function of time is determined by Eq. (17). The factors affecting the spring specific pressure are the amplitude and period of the spring alternating load. When studying the influence of alternating load on mechanical seal, set the boundary pressure of inlet and outlet to be stable, that is, the inlet pressure is 0.1 MPa and the outlet pressure is 0.15 MPa.

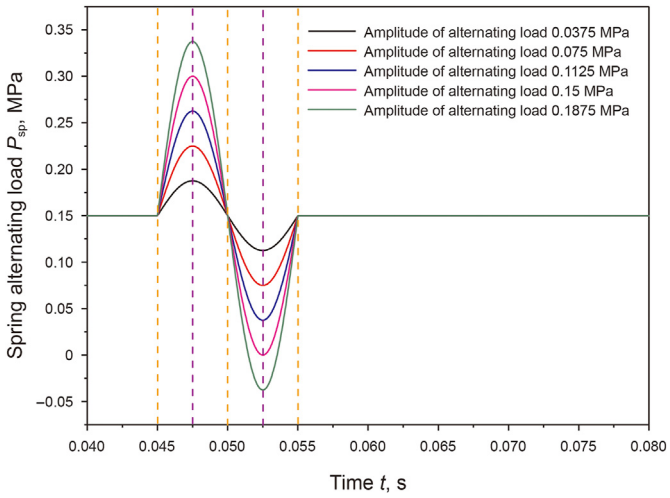

Fig. 22. Variation of spring alternating load with time.

The variation of spring alternating load with time is shown in Fig. 22. The load amplitude is taken as 0.0375, 0.075, 0.1125, 0.15 and 0.1875 MPa, the action time of alternating load is 0.01 s, and the calculation to 0.08 s at the end of load disturbance can ensure that the compensation ring will restore stability when it reaches the end of calculation.

The change of film thickness with time is shown in Fig. 23(a), and the alternating load also causes the film thickness to exhibit alternating characteristics (Yan et al., 2012). The change of alternating load is approximately negatively correlated with the change of film thickness, that is, the alternating load increases and the film thickness decreases, but there is still a phase difference between the film thickness and the alternating load of the spring. As the amplitude of the load increases, the change in film thickness becomes greater. Compared with the influence of inlet pressure disturbance on film thickness, the change in film thickness is greater under alternating load. This is because the pressure disturbance condition changes the fluid force by changing the internal pressure of the flow field, while alternating load directly acts on the sealing ring by changing the closing force. The variation of liquid film cavitation rate with time is shown in Fig. 23(b). When the load amplitude is greater than 0.15 MPa, there is a time period when the liquid film cavitation rate is 0, that is, there is no cavitation in the mechanical seal liquid film. The liquid film cavitation rate reaches the maximum value at 0.52 s, and the peak value at 0.1875 MPa is about 2.35%. The change of pressure at measuring point with time is shown in Fig. 24. The change trend of pressure at measuring point A is basically consistent with the change of alternating load. The difference is that there is hysteresis, and there is a recovery period of end face pressure at the end of disturbance. When the amplitude is 0.1125, 0.15 and 0.1875 MPa, the pressure of measuring point B remains unchanged during 0.05–0.055 s. When the amplitude is 0.1875 MPa, the pressure at measuring point C will increase sharply, and the end face cavitation will disappear, which is caused by the increase of pressure in the low-pressure area.

Further explore the change of axial speed and leakage with time,

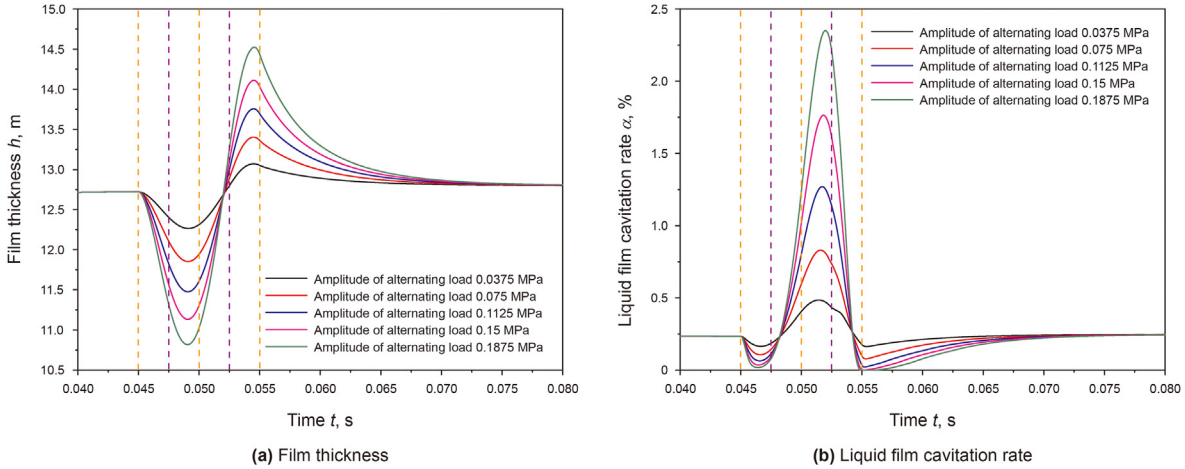

(a) Film thickness **(b)** Liquid film cavitation rate

Fig. 23. Variation of film thickness and liquid film cavitation rate with time.

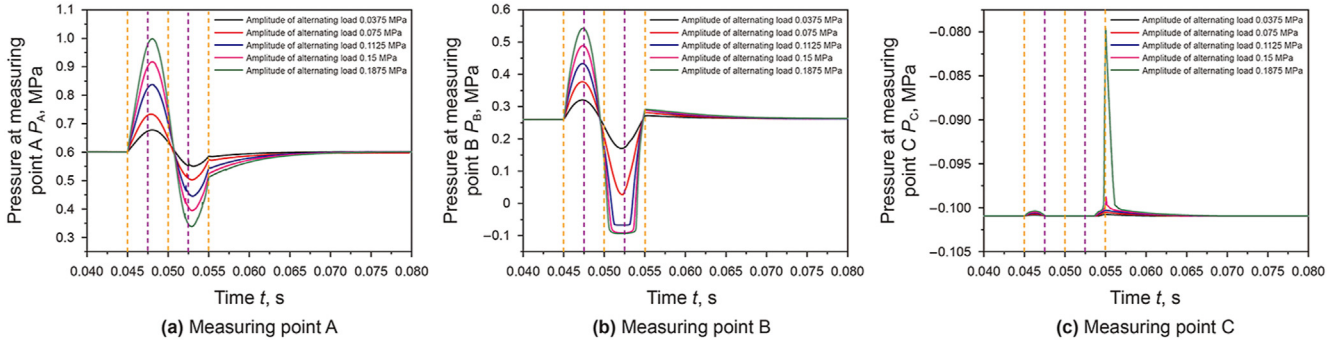

(a) Measuring point A **(b)** Measuring point B **(c)** Measuring point C

Fig. 24. Pressure change of measuring point with time.

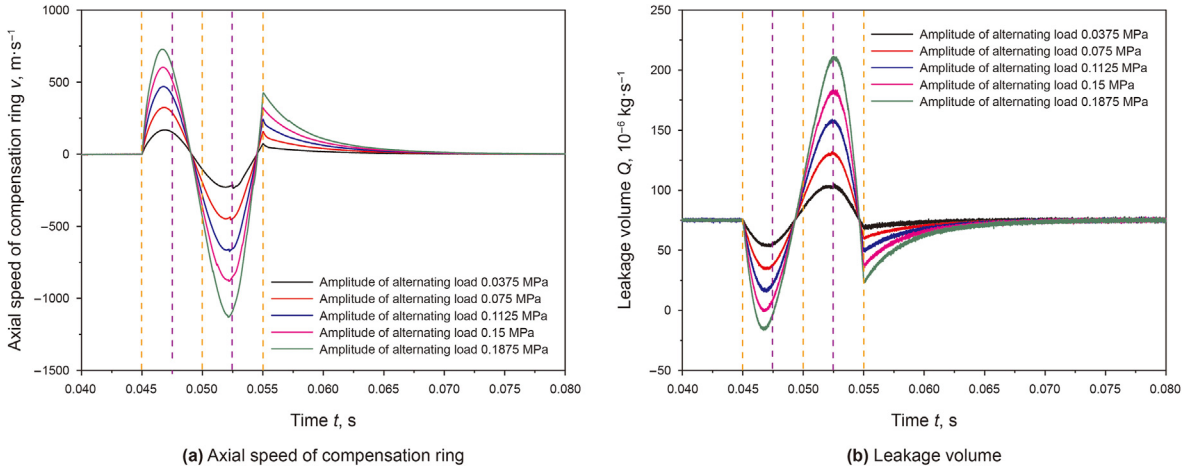

(a) Axial speed of compensation ring **(b)** Leakage volume

Fig. 25. Variation of axial speed and leakage of compensation ring with time.

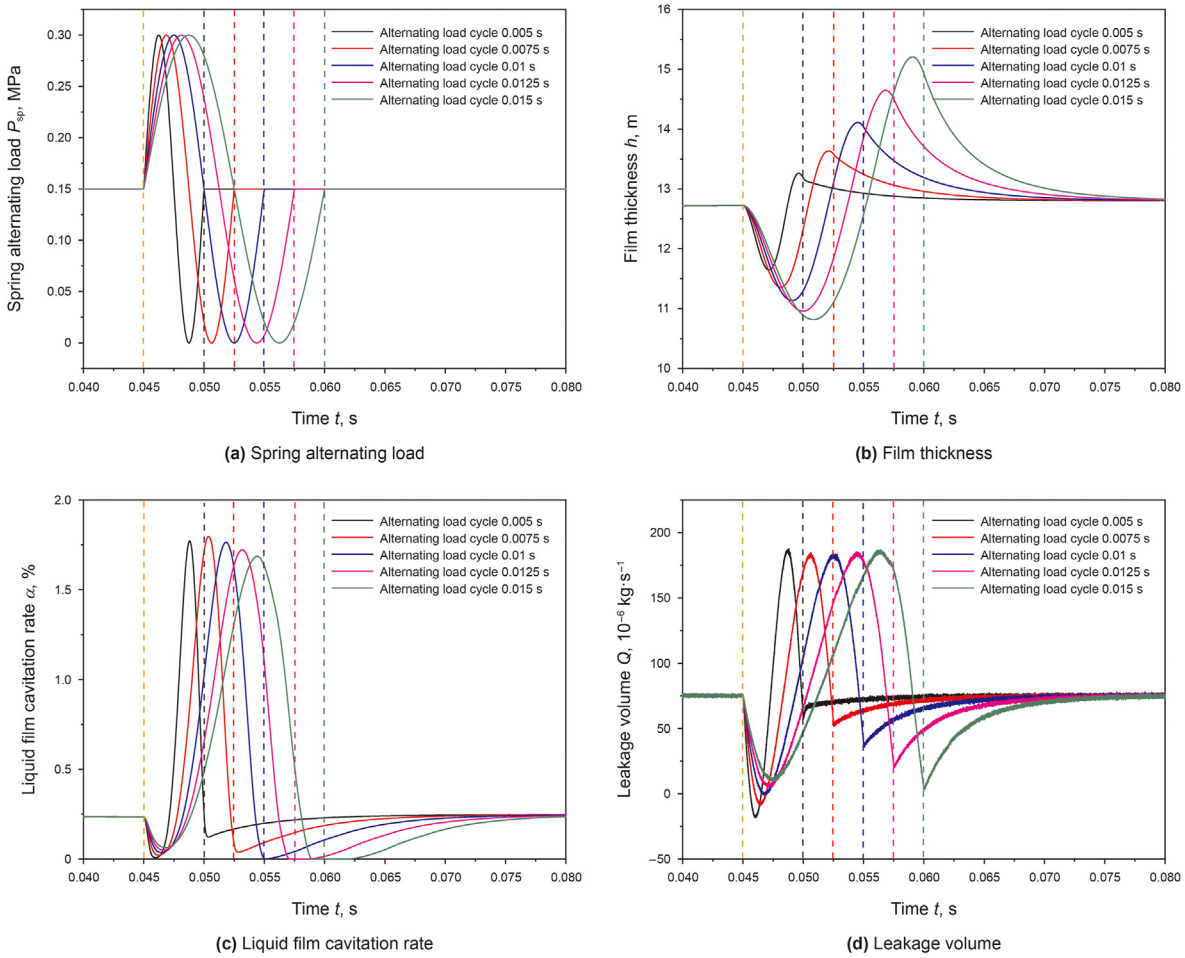

(a) Spring alternating load **(b)** Film thickness

(c) Liquid film cavitation rate **(d)** Leakage volume

Fig. 26. Variation of spring alternating load, film thickness, liquid film cavitation rate and leakage with time.

as shown in Fig. 25. The maximum speed in axial speed is about −1100 μm/s, the displacement per unit time step is about 2.2×10^{-3} μm. With the increase of load amplitude, the peak value of axial velocity also increases gradually. Compared with Fig. 25(b), it is found that the change of axial speed is in inverse phase with the change of leakage, that is, the phase difference is π, which is consistent with the disturbance of inlet pressure. Under the action of alternating load, the change of leakage volume increases significantly, and the peak value appears at 0.0525 s, and the time of the peak value is independent of the load amplitude. When the load amplitude is 0.1875 MPa, the maximum leakage is about 210 mg/s.

4.2.2. *Influence of load cycle on compensation ring*

Further explore the influence of different alternating load cycles

on the dynamic response characteristics of liquid film seal. The variation of alternating load with time is shown in Fig. 26(a). The load cycles are 0.005, 0.0075, 0.01, 0.0125 and 0.015 s, the amplitude of alternating load is 0.15 MPa, and the calculation time is 0.08 s. The film thickness changes with time, as shown in Fig. 26(b). With the increase of load cycle, the peak value of film thickness in the disturbance process gradually increases. Compared with the influence of pressure disturbance period on the compensation ring, the influence of alternating load period on the compensation ring is greater. When the load cycle is 0.015 s, the difference between the minimum film thickness and the maximum film thickness is about 4.5 μm. However, the load cycle has little effect on the maximum value of liquid film cavitation rate and leakage, as shown in Fig. 26(c) and (d). As the load cycle increases, the time when the liquid film cavitation rate is 0 gradually increases. However, at the end of the disturbance, the increase of the alternating load cycle leads to the disappearance of cavitation and the reduction of leakage. The change of the pressure at the measuring point is basically consistent with the influence law of the pressure disturbance period on the pressure at the measuring point, which is not repeated here.

5. Conclusion

The dynamic characteristics and sealing performance of mechanical seal for gas-liquid multiphase pump under complex working conditions are studied. Based on the fluid solid coupling theory, the reciprocating motion of liquid film seal under unstable working conditions is realized. The influence of pressure disturbance and alternating load at the inlet under the change of trigonometric function on the vibration characteristics of compensation ring is explored. The main conclusions are as follows.

(1) The amplitude and period of pressure disturbance at the inlet have an impact on the change of film thickness. With the increase of disturbance amplitude and period, the film thickness gradually decreases, while the cavitation rate of liquid film gradually increases. The hysteresis of film thickness change is caused by the damping effect of liquid film, and the fundamental reason is that the pressure in the high-pressure area cannot be restored in time. There is a close relationship between leakage and axial velocity. The phase difference between the two is π. The maximum value of leakage and the minimum value of axial velocity are independent of the disturbance period and are determined by the disturbance amplitude.

(2) The stable disturbance wave can promote the reduction of film thickness, and the compensation ring vibrates slightly when the liquid film thickness is 12.3 μm. With a small range of pressure disturbance, the influence of the interference between the enhanced waves on the film thickness is not obvious, while the front wave in the attenuated wave promotes the film thickness change at the later time. Under the condition of enhanced wave, the liquid film cavitation rate and axial velocity fluctuate near the initial value, while under the condition of attenuated wave, the fluctuation of liquid film cavitation rate and axial velocity deviates from the initial value.

(3) Compared with the pressure disturbance condition, the alternating load condition changes the film thickness and leakage more significantly, and its influence on various parameters is basically the same as that under the pressure disturbance condition. During the movement of the compensation ring, there is a period when the liquid film cavitation rate is 0, and with the increase of the load cycle, the time when the liquid film cavitation rate is 0 is longer.

(4) Based on the study of the influence of the pressure disturbance wave at the inlet on the mechanical seal, the dynamic characteristics and sealing performance changes of the liquid film seal compensation ring under the condition of long-term pressure disturbance can be further predicted. The mechanical seal for multiphase pump should avoid the occurrence of alternating load in the actual operation process to ensure the stability of the mechanical seal and small leakage.

CRediT authorship contribution statement

Qing-Ping Li: Conceptualization, Data curation, Formal analysis, Investigation, Methodology, Writing – original draft. **Jin-Ya Zhang:** Data curation, Formal analysis, Funding acquisition, Investigation, Methodology. **Jia-Xiang Zhang:** Conceptualization, Data curation, Formal analysis, Investigation, Methodology, Software, Writing – original draft. **Yong-Xue Zhang:** Formal analysis, Investigation, Methodology.

Declaration of competing interest

There are no conflicts of interest with other people or organizations that may inappropriately influence the author's actions.

Acknowledgments

The authors would like to acknowledge the support of the National Natural Science Foundation of China (52372368).

Nomenclature

Abbreviations

IGVF	Inlet gas phase volume fraction
GVF	Gas phase volume fraction
FSI	Fluid-structure interaction
in	Inlet
out	Outlet
max	Maximum
Tem	Temperature

Main Symbols

r	Seal face semidiameter
e	Constant
h_c	Spiral groove depth
h_0	Initial film thickness
h_b	Balance film thickness
h_a	Assumed film thickness
N	Number of spiral grooves
n	Speed
T	Fluctuation period
t	Time
R_c	Bubble collapse term
R_e	Bubble generation term
P_1	Pressure, constant
P_0	Pressure, half of fluctuation amplitude
P_{sp}	Spring pressure
Q	Leakage volume
F_p	Fluid force
K	Axial stiffness
D	Axial damping

m	Mass of compensation ring
F_{cls}	Closing force
F	Combined external force

Greek letters

φ	Helix expansion angle
θ	Helix angle
β	Groove semidiameter ratio
γ	Groove width ratio
α	Liquid film cavitation rate
μ	Viscosity coefficient
π	Constant
ω	Angular frequency
ρ	Medium density
ω_0	Natural frequency
ξ	Structural damping

Subscripts

i	i direction in space
j	j direction in space
m	Average value
v	Gas phase
l	Liquid phase

References

Blasiak, S., Zahorulko, A., 2016. A parametric and dynamic analysis of non-contacting gas face seals with modified surfaces. Tribol. Int. 94 (2), 126–137. https://doi.org/10.1016/J.TRIBOINT.2015.08.014.

Chen, M., 2006. Fundamentals of Viscous Fluid Dynamics. Higher Education Press, Beijing, pp. 34–50.

Chen, H., Fu, J., Li, S., et al., 2015. Pressure fluctuation characteristic of mechanical face sealing clearance of spiral groove in upstream pumping. Journal of Drainage and Irrigation Machinery Engineering 33 (6), 504–509. https://doi.org/10.3969/j.issn.1674-8530.14.0189.

Chen, Y., Jiang, J., Peng, X., 2017. Dynamic characteristics and transient sealing performance analysis of hyperelliptic curve groove dry gas seals. Tribol. Int. 116 (12), 217–228. https://doi.org/10.1016/J.TRIBOINT.2017.07.017.

Childs, D., 2018. A new structural dynamic model for pump mechanical seals vibration analysis incorporating squeeze motion of O-ring seals and general dynamic motion of the pump housing and the pump shaft. J. Tribol. 140 (6), 062201. https://doi.org/10.1115/1.4038867.

Concli, F., 2016. Pressure distribution in small hydrodynamic journal bearings considering cavitation: a numerical approach based on the open-source CFD code OpenFOAM®. Lubric. Sci. 28 (6), 329–347. https://doi.org/10.1002/ls.1334.

Cochain, J., Brunetiere, N., Parry, A., et al., 2020. Experimental and numerical study of wavy mechanical face seals operating under pressure inversions. Proc. IME J. J. Eng. Tribol. 234 (2), 247–260. https://doi.org/10.1177/1350650119862696.

Etison, I., Burstein, L., 1996. A model for mechanical seals with regular micro-surface structure. Tribol. Trans. 39 (3), 667–683. https://doi.org/10.1080/10402009608983582.

Findlay, J., 1968. Cavitation in mechanical face seals. Journal of Lubrication Technology 90 (2), 356–364. https://doi.org/10.1115/1.3601569.

Green, I., Izhak, E., 1983. Fluid film dynamic coefficients in mechanical face seals. Journal of Lubrication Technology 105 (4), 297–302. https://doi.org/10.1115/1.3254596.

Green, I., Barnsby, R., 2001. A simultaneous numerical solution for the lubrication and dynamic stability of non-contacting gas face seals. J. Tribol. 123 (2), 388–394. https://doi.org/10.1115/1.1308020.

Hao, M., Wang, Y., Li, Z., et al., 2018. Effects of surface topography on hydrodynamic performance of liquid film seals considering cavitation. Ind. Lubric. Tribol. 70 (6), 984–992. https://doi.org/10.1108/ILT-12-2016-0321.

Jiang, S., Ji, H., Wang, T., et al., 2019. Enhanced understanding of leakage in mechanical seals with elliptical dimples based on CFD simulation. Ind. Lubric. Tribol. 72 (1), 24–30. https://doi.org/10.1108/ilt-03-2019-0087.

Li, Z., Liu, Z., Lv, Y., et al., 2015. Numerical investigation on altitude performance for aeroengine gerotor pump. J. Propuls. Technol. 36 (6), 846–851. https://doi.org/10.13675/j.cnki.tjjs.2015.06.007.

Li, Y., Hao, M., Sun, X., et al., 2019. 3-DOF dynamic response characteristics of rotor compensated liquid film seal. J. Vib. Shock 38 (1), 50–57. https://doi.org/10.13465/j.cnki.jvs.2019.01.008.

Li, Z., Hao, M., Sun, X., et al., 2020a. Experimental study of cavitation characteristic of single-row reverse spiral groove liquid-film seals. Tribol. Int. 141 (1), 105782. https://doi.org/10.1016/J.TRIBOINT.2019.05.022.

Li, Y., Hao, M., Sun, X., et al., 2020b. Dynamic response of spiral groove liquid film seal to impact conditions. Tribol. Int. 141 (7), 105865. https://doi.org/10.1016/J.TRIBOINT.2019.105865.

Li, Z., Li, Y., Cao, H., et al., 2021. Investigation of cavitation evolution and hydrodynamic performances of oil film seal with spiral groove. Tribol. Int. 157 (7), 106915. https://doi.org/10.1016/J.TRIBOINT.2021.106915.

Mayer, E., 1977. Mechanical Seals. Newnes-Butterworths, London.

Meng, X., Khonsari, M., 2017. On the effect of viscosity wedge in micro-textured parallel surfaces. Tribol. Int. 107 (3), 116–124. https://doi.org/10.1016/J.TRIBOINT.2016.11.007.

Meng, X., Khonsari, M., 2018. Viscosity wedge effect of dimpled surfaces considering cavitation effect. Tribol. Int. 122 (6), 58–66. https://doi.org/10.1016/J.TRIBOINT.2018.02.011.

Nau, B., 1980. Observations and analysis of mechanical seal film characteristics. Journal of Lubrication Technology 102 (3), 341–347. https://doi.org/10.1115/1.3251534.

Necker, N., 2003. Mechanical sealing technology used in multiphase production. J. Can. Petrol. Technol. 42 (9), 28–31. https://doi.org/10.2118/03-09-N2.

Peng, X., Jin, J., Meng, X., et al., 2019. Research progress on the liquid face seal of vapor-liquid two-phase flow. Tribology 39 (5), 643–655. https://doi.org/10.16078/j.tribology.2018093.

Rouillon, M., Noël, B., 2018. Spiral groove face seal behavior and performance in liquid lubricated applications. Tribol. Trans. 61 (7), 1048–1056. https://doi.org/10.1080/10402004.2018.1463426.

Sun, X., Meng, X., Zhou, G., et al., 2017. Analysis of thermal-mechanical coupling characteristics on seal faces under alternative load function. Lubr. Eng. 42 (8), 48–53. https://doi.org/10.3969/j.issn.0254-0150.2017.08.009.

Sun, D., Sun, J., Ma, C., et al., 2019. Frequency-domain based nonlinear response analysis of stationary ring displacement of noncontact mechanical seal. Shock Vib., 7082538. https://doi.org/10.1155/2019/7082538.

Shi, G., Liu, Z., Xiao, Y., et al., 2020. Tip leakage vortex trajectory and dynamics in a multiphase pump at off-design condition. Renew. Energy 150 (5), 703–711. https://doi.org/10.1016/j.renene.2020.01.024.

Tokunaga, Y., Inoue, H., Okada, K., et al., 2011. Effects of cavitation ring formed on laser-textured surface of mechanical seal. Tribol. Online 6 (1), 36–39. https://doi.org/10.2474/TROL.6.36.

Xue, B., Wei, C., Hu, J., 2017. Study of separation characteristics of micro-groove rotary seal considering different cavitation boundary conditions. Tribol. Lett. 65 (4), 119. https://doi.org/10.1007/s11249-017-0893-x.

Xu, L., Wu, J., Wang, Y., et al., 2020. Transient response and rub-impact phenomenon of liquid lubricated non-contacting mechanical seals during external pressure fluctuation. J. Braz. Soc. Mech. Sci. Eng. 42 (7), 1–11. https://doi.org/10.1007/s40430-020-02485-1.

Yan, G., Liu, Z., 2012. Transient coupling characteristics study on mechanical seals end faces under the alternative loads function. Chin. J. Comput. Mech. 29 (4), 551–555.

Yang, W., 2019. Study on Dynamic Characteristics of Liquid Film Seal Based on Cavitation Effect. PhD Thesis. China University of Petroleum (East China).

Zeus, D., 1993. Cavitation-a little noticed factor in the operation of mechanical seals. Ind. Lubric. Tribol. 45 (2), 3–6. https://doi.org/10.1108/EB053424.

Zhou, J., Fan, H., Shao, C., 2016. Experimental study on the hydrodynamic lubrication characteristics of magnetofluid film in a spiral groove mechanical seal. Tribol. Int. 95 (3), 192–198. https://doi.org/10.1016/J.TRIBOINT.2015.11.018.

Zhang, J., Zhang, J., Li, Q., et al., 2022a. Effect of pressure fluctuation in oil-gas multiphase pump on cavitation and performance of sealing liquid film. J. Petrol. Sci. Eng. 210 (3), 110074. https://doi.org/10.1016/j.petrol.2021.110074.

Zhang, J., Zhang, J., Zhou, Y., et al., 2022b. Investigation on the performance of a helico-axial multiphase pump under slug flow. Petrol. Sci. 19 (4), 1812–1824. https://doi.org/10.1016/j.petsci.2021.10.031.